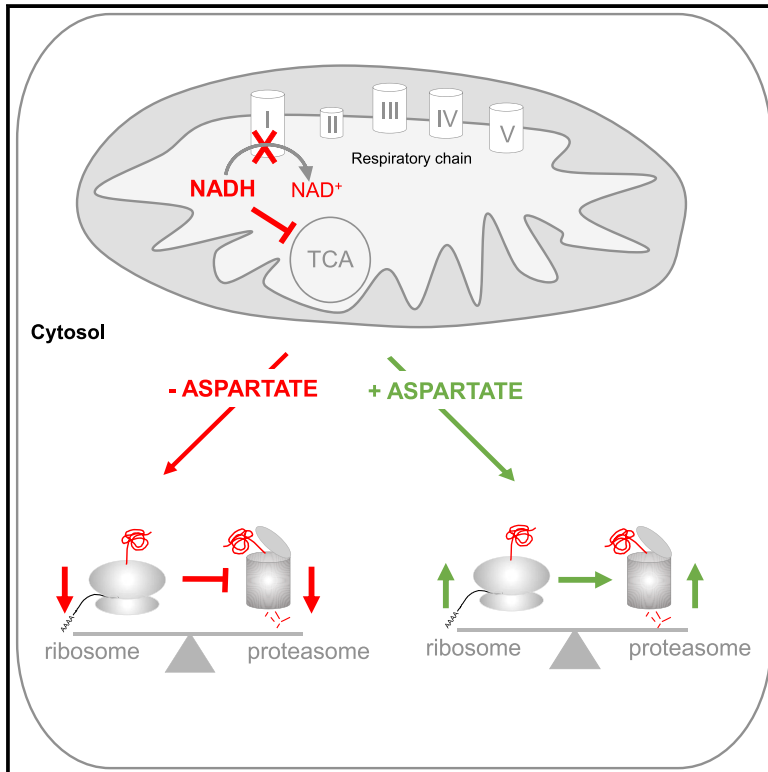


Mitochondrial Regulation of the 26S Proteasome

Graphical Abstract



Authors

Thomas Meul, Korbinian Berschneider, Sabine Schmitt, ..., Stefanie M. Hauck, Hans Zischka, Silke Meiners

Correspondence

silke.meiners@helmholtz-muenchen.de

In Brief

Meul et al. demonstrate reversible regulation of 26S proteasome assembly and activity by metabolic reprogramming of the TCA cycle upon impaired respiratory function. Supplementation with aspartate or pyruvate restores 26S proteasome activity via mTORC1-mediated transcriptional activation of defined proteasome assembly factors.

Highlights

- Respiratory dysfunction impairs 26S proteasome assembly and activity
- Aspartate deficiency inhibits protein synthesis and 26S proteasome activity via mTORC1
- Aspartate restores 26S activity via upregulation of proteasome assembly factors
- Addition of pyruvate overcomes resistance to bortezomib in respiration-deficient cells



Article

Mitochondrial Regulation of the 26S Proteasome

Thomas Meul,¹ Korbinian Berschneider,¹ Sabine Schmitt,^{2,10} Christoph H. Mayr,¹ Laura F. Mattner,¹ Herbert B. Schiller,¹ Ayse S. Yazgili,¹ Xinyuan Wang,¹ Christina Lukas,¹ Camille Schlessner,¹ Cornelia Prehn,³ Jerzy Adamski,^{3,13,14} Elisabeth Graf,⁴ Thomas Schwarzmayr,⁴ Fabiana Perocchi,^{5,12} Alexandra Kukat,⁶ Aleksandra Trifunovic,⁶ Laura Kremer,⁷ Holger Prokisch,^{7,15} Bastian Popper,^{8,9} Christine von Toerne,¹⁰ Stefanie M. Hauck,¹⁰ Hans Zischka,^{2,11} and Silke Meiners^{1,16,*}

¹Member of the German Center for Lung Research (DZL), Comprehensive Pneumology Center (CPC), University Hospital, Ludwig-Maximilians University, Helmholtz Zentrum München, 81377 Munich, Germany

²Institute of Toxicology and Environmental Hygiene, Technical University of Munich, School of Medicine, 80802 Munich, Germany

³Research Unit Molecular Endocrinology and Metabolism, Genome Analysis Center, Helmholtz Zentrum München, German Research Center for Environmental Health, Ingolstädter Landstraße 1, 85764 Neuherberg, Germany

⁴Institute of Human Genetics, Core Facility Next-Generation-Sequencing, Helmholtz Zentrum München, 85764 Munich, Germany

⁵Institute for Diabetes and Obesity, Helmholtz Diabetes Center (HDC), Helmholtz Zentrum München, 85764, Neuherberg, Germany

⁶Cologne Excellence Cluster on Cellular Stress Responses in Ageing-Associated Diseases (CECAD), Medical Faculty, University of Cologne, D-50931 Cologne, Germany

⁷Institute of Neurogenomics, Helmholtz Zentrum München, 85764 Neuherberg, Germany

⁸Biomedical Center, Core facility animal models, Ludwig-Maximilian-University Munich, 82152 Martinsried, Germany

⁹Institute of Pathology, School of Medicine, Technical University of Munich, 81675 Munich, Germany

¹⁰Research Unit Protein Science, Helmholtz Zentrum München, 80939 Munich, Germany

¹¹Institute of Molecular Toxicology and Pharmacology, Helmholtz Zentrum München, 85764 Neuherberg, Germany

¹²Munich Cluster for Systems Neurology, 81377, Munich, Germany

¹³Lehrstuhl für Experimentelle Genetik, Technische Universität München, 85350 Freising-Weihenstephan, Germany

¹⁴Department of Biochemistry, Yong Loo Lin School of Medicine, National University of Singapore, 8 Medical Drive, Singapore 117597, Singapore

¹⁵Institute of Human Genetics, Technical University of Munich (TUM), School of Medicine, 81675 Munich, Germany

¹⁶Lead Contact

*Correspondence: silke.meiners@helmholtz-muenchen.de

<https://doi.org/10.1016/j.celrep.2020.108059>

SUMMARY

The proteasome is the main proteolytic system for targeted protein degradation in the cell and is fine-tuned according to cellular needs. Here, we demonstrate that mitochondrial dysfunction and concomitant metabolic reprogramming of the tricarboxylic acid (TCA) cycle reduce the assembly and activity of the 26S proteasome. Both mitochondrial mutations in respiratory complex I and treatment with the anti-diabetic drug metformin impair 26S proteasome activity. Defective 26S assembly is reversible and can be overcome by supplementation of aspartate or pyruvate. This metabolic regulation of 26S activity involves specific regulation of proteasome assembly factors via the mTORC1 pathway. Of note, reducing 26S activity by metformin confers increased resistance toward the proteasome inhibitor bortezomib, which is reversible upon pyruvate supplementation. Our study uncovers unexpected consequences of defective mitochondrial metabolism for proteasomal protein degradation in the cell, which has important pathophysiological and therapeutic implications.

INTRODUCTION

The ubiquitin-proteasome system is a central part of cellular protein homeostasis. It recycles amino acids for protein synthesis, maintains protein quality control, and controls the half-life of essential regulators of cell function (Finley, 2009; Fredrickson and Gardner, 2012; Vabulas and Hartl, 2005). Ubiquitin-dependent protein degradation is carried out by 26S proteasome complexes (Ciechanover, 2015). The 26S proteasome consists of a central catalytic core—the 20S proteasome—with one or two 19S regulators attached to the ends of the 20S forming single- or double-capped 26S proteasome complexes (Bard et al.,

2018). While the 20S proteasome core contains the three proteolytic sites with chymotrypsin-, caspase-, and trypsin-like activities for protein hydrolysis, the 19S regulator mediates ATP-dependent binding and unfolding of ubiquitinated substrates as well as recycling of ubiquitin moieties (Bard et al., 2018).

Mitochondria are the powerhouses of the cell, providing energy and redox equivalents via their respiratory chain (Spinelli and Haigis, 2018). Besides ATP production via the respiratory chain, mitochondria play key metabolic functions in the biosynthesis of nucleotides, lipids, and amino acids by generating essential intermediates via the TCA (tricarboxylic acid) cycle (Ahn and Metallo, 2015). Dysfunction of the respiratory chain



results in defective ATP production and metabolic reprogramming of the cell due to imbalanced redox equivalents (Birsoy et al., 2015; Sullivan et al., 2015, 2016).

Mitochondrial function is coupled to the ubiquitin-proteasome system (D'Amico et al., 2017; Livnat-Levanon and Glickman, 2011; Segref et al., 2014). Proteins of the inner and outer mitochondrial membrane are degraded in a ubiquitin-dependent manner by the 26S proteasome (Karbowsky and Youle, 2011; Lavie et al., 2018). Accumulation of misfolded or mistargeted mitochondrial proteins results in the adaptive activation of the ubiquitin-proteasome system to maintain mitochondrial and cellular proteostasis (Münch and Harper, 2016; Suhm et al., 2018; Wang and Chen, 2015; Wrobel et al., 2015). Conversely, 26S proteasome activity is reduced by defective ATP production after acute pharmacological inhibition of respiratory chain complexes (Höglinger et al., 2003) and 26S proteasome complexes disassemble upon excessive production of mitochondrial reactive oxygen species (ROS; Chou et al., 2010; Livnat-Levanon et al., 2014; Segref et al., 2014). On the other hand, defective proteasome function is compensated by adaptations of the mitochondrial metabolism (Tsvetkov et al., 2019).

We here demonstrate reversible fine-tuning of 26S proteasome activity by metabolic reprogramming of the cell. Specifically, we show that defective respiratory complex I function impairs the assembly of the 26S proteasome, which can be alleviated upon addition of aspartate or pyruvate. Assembly of 26S proteasome complexes depends on aspartate-mediated regulation of the mammalian target of rapamycin (mTOR) complex 1 (mTORC1) pathway and subsequent transcriptional upregulation of specific proteasome assembly factors. Thus, our study uncovers a fundamental cell biological mechanism of adjusting protein degradation by the proteasome to the metabolic program of the cell, which has pathophysiological but also therapeutic consequences.

RESULTS

Respiratory Chain Dysfunction Reduces 26S Proteasome Activity and Assembly

We set out to study metabolic regulation of proteasome activity in a model system of genetically impaired respiratory function without oxidative stress using mouse embryonic fibroblasts (MEFs) of DNA mutator mice. These cells express a proof-reading-deficient mutant of the mitochondrial DNA polymerase γ and accumulate random point mutations in their mitochondrial DNA (mtDNA), resulting in almost complete loss of respiratory chain activity (Figures S1A and S1B). While mutator cells grew slower, they did not show any morphological signs of stress (Figures S1C and S1D). Experiments were performed with four different mutator and three distinct wild-type (WT) MEF cell lines to minimize clonal differences in the accumulation of mitochondrial DNA mutations (Edgar et al., 2009).

The activity of all three proteolytic sites of the proteasome, namely the chymotrypsin-, caspase-, and trypsin-like activities, was uniformly diminished in mutator cells when assaying specific substrate degradation (Figure 1A). We did not observe any differences in the expression of proteasomal subunits in WT and mutator cells (Figure 1B). Western blot analysis for

20S alpha and beta 5 subunits and for the 19S regulator subunits Rpn8 and Rpt5 revealed similar expression levels. This finding was confirmed for RNA expression by RNA sequencing (Figure 1C; Table S1) and quantitative reverse transcriptase PCR (qRT-PCR) analysis for selected proteasome encoding genes (Figure S1E). For an overview on the divergent protein and gene names of proteasomal subunits, the reader is referred to Wang et al. (2020). We next used native gels with substrate overlay analysis and immunoblotting to resolve the different active proteasome complexes in the cell. This method allows the discrimination into 20S proteasomes and single- (26S) and double-capped (30S) proteasome complexes. Cells with mitochondrial dysfunction showed reduced activity and amount of assembled single- and double-capped 26S proteasome complexes, whereas the level of free 20S proteasomes was slightly but not significantly increased (Figure 1D). The total amount of 20S complexes was marginally decreased in mutator compared to WT cells (Figure S1F). This coincided with reduced levels of the 20S assembly factor Pom1 in mutator cells (Figure S1G).

26S proteasome deficiency in mutator cells might be caused by disassembly of 26S complexes into 20S catalytic core particles and 19S regulators due to diminished ATP or elevated ROS levels (Höglinger et al., 2003; Livnat-Levanon et al., 2014). Cellular ATP levels, however, were not reduced despite impaired mitochondrial ATP production (Figure S1H)—indicating maintenance of ATP production via elevated rates of glycolysis in mutator cells, as suggested by the reduced spare glycolytic capacity of the mutator cells (Figure S1I), and as described before (Saleem et al., 2015). ROS levels were not increased in mutator cells as determined by cellular DCF (2', 7' -dichlorofluorescein) and mitochondrial superoxide (mitoSOX) fluorescence (Figure S1J), confirming previous results (Trifunovic et al., 2005). To also exclude effects of ROS micro-signaling, cells were treated with the antioxidant N-acetylcysteine (NAC). Proteasome activity in mutator cells was, however, not rescued by NAC treatment (Figure S1K). These data indicate that reduced formation of 26S proteasome complexes in mutator cells does not involve ROS-mediated disassembly but rather reduced assembly of 26S proteasome complexes. We also did not observe any signs of protein stress in our proteomic comparison of WT and mutator cells (Tables S2 and S8). Reduced activity of the 26S proteasome did not alter the turnover of ubiquitinated proteins in mutator cells, as levels of K48 polyubiquitinated proteins were similar to WT cells (Figure S1L). These findings suggest that reduced assembly of 26S proteasome complexes is part of an adaptive proteostatic cell response to mitochondrial dysfunction.

Respiratory Chain Dysfunction Results in Aspartate Deficiency

To elucidate the molecular mechanism involved in reduced 26S proteasome function in cells with mitochondrial dysfunction, we investigated the nature of mitochondrial alterations in mutator cells in detail. Cytochrome c staining revealed that neither the mitochondrial network nor mitochondria numbers were substantially altered in mutator compared to WT cells (Figure 2A, upper panel). We further purified intact mitochondria according to our recently developed protocol (Schmitt et al., 2015) and as

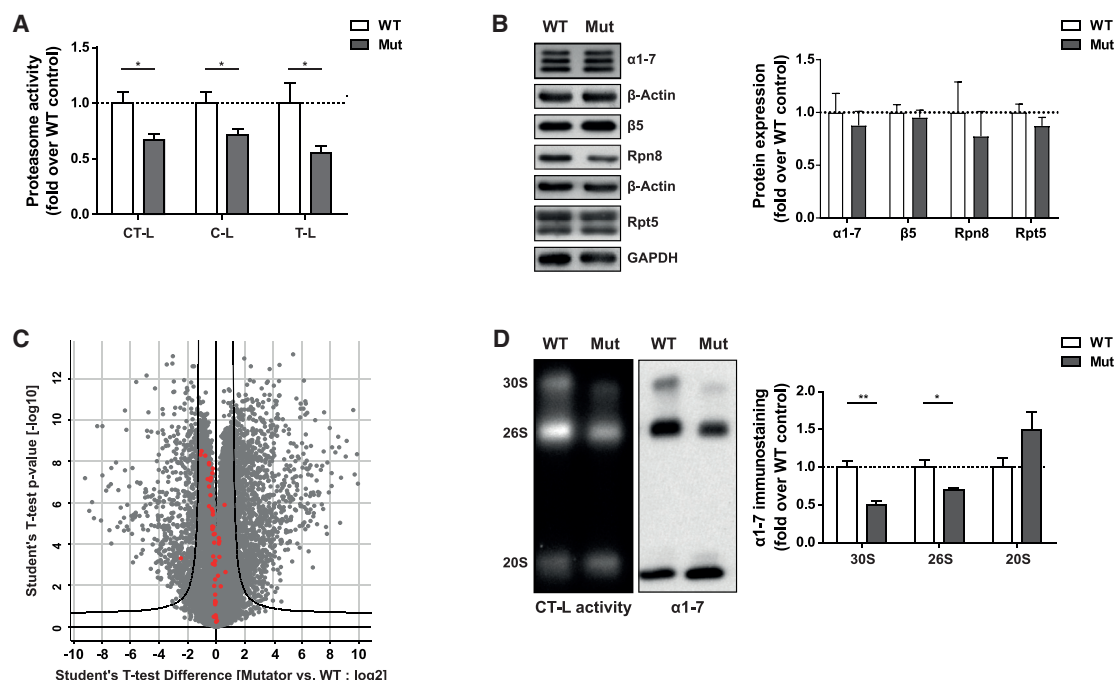


Figure 1. Respiratory Chain Dysfunction Reduces 26S Proteasome Activity and Assembly

(A) Proteasome activity in total cell extracts of WT ($n = 3$) and mutator (Mut; $n = 4$) cells as measured by cleavage of luminogenic substrates specific for the chymotrypsin-like (CT-L), caspase-like (C-L), or trypsin-like (T-L) active sites of the proteasome. Bar graphs show mean \pm SEM relative to WT MEFs. Significance was determined using two-way ANOVA with a Bonferroni multiple comparison test.

(B) Representative western blot analysis of 20S ($\alpha 1-7$, $\beta 5$) and 19S regulator (Rpn8, Rpt5) subunit expression in WT and Mut cells. β -actin or GAPDH were used as loading controls. Densitometric analysis shows mean \pm SEM from three WT and four Mut cell lines. Statistical test: Student's unpaired t test.

(C) Volcano plot showing mRNA expression levels as identified by mRNA bulk sequencing of one WT ($n = 4$ technical replicates) and one Mut ($n = 5$ technical replicates) cell line using a 1% false discovery rate (FDR), which is indicated by the black lines. mRNA levels of proteasome subunits are shown in red.

(D) Representative native gel analysis of active proteasome complexes and quantification thereof from native cell lysates from WT ($n = 3$) and Mut ($n = 4$) cells with CT-L substrate overlay assay and immunoblotting for 20S $\alpha 1-7$ subunits. The resolution of double-capped (30S) and single-capped 26S proteasomes (26S) is indicated together with the 20S proteasome complexes (20S). Bar graphs show mean \pm SEM relative to WT MEFs. Significance was determined using Student's unpaired t test comparing WT versus Mut cells.

See also [Figure S1](#) and [Tables S2](#) and [S8](#).

schematically depicted in [Figure S2A](#). Mitochondria of mutator cells were structurally intact, with only slight alterations in mitochondrial cristae structures, as shown by electron microscopy of both cellular and isolated mitochondria ([Figures 2A](#), lower panel and [S2B](#)). To confirm that the number of mitochondria is similar in WT and mutator cells, the proportion of mitochondrial volume was quantified as described by [Hacker and Lucocq \(2014\)](#) ([Figure S2C](#)). Proteomic analysis of isolated mitochondria from WT and mutator cells identified 714 mitochondrial proteins according to MitoCarta 2.0 ([Calvo et al., 2016](#); [Table S3](#)). More than 90% of these mitochondrial proteins were not regulated more than twofold. Using enrichment analysis on UniProt keywords and gene-ontology terms, we observed severe downregulation of respiratory chain proteins ([Figure 2B](#); [Tables S3](#) and [S4](#)). These mapped mainly to complex I and complex IV, as confirmed by immunoblot analysis ([Figure S2D](#)). Complex I deficiency and the resulting lack of electron transfer resulted in impaired oxidation of NADH to NAD^+ and pronounced accumulation of NADH in mutator cells ([Figure 2C](#)). Elevated NADH levels inhibit key enzymes of the TCA cycle ([Chandel, 2015a](#)). Together with the lack of NAD^+

electron acceptors, this hampers production of TCA cycle intermediates that are required for the biosynthesis of macromolecules, such as amino acids ([Figure 2D](#); [Chandel, 2015b](#); [Sullivan et al., 2015](#)). Metabolomic quantification of amino acid levels revealed that the amount of aspartate was significantly decreased in mutator cells, whereas overall levels of amino acids were not altered ([Figures 2E](#) and [S2E](#); [Table S5](#)). As aspartate is not supplemented in cell culture medium ([Dulbecco and Freeman, 1959](#)), cells strictly depend on the endogenous biosynthesis of aspartate for subsequent generation of amino acids, purines, and pyrimidines ([Birsoy et al., 2015](#); [Fu and Danial, 2018](#); [Sullivan et al., 2015](#)). Our analysis thus identifies deficiency of complex I, concomitant loss of electron acceptors, and reduced levels of aspartate as major features of metabolic reprogramming in mutator cells.

Supplementation of Aspartate Activates 26S Proteasome Activity

We next tested whether the observed aspartate deficiency in mutator cells contributes to the impairment of 26S proteasome activity. Of note, aspartate supplementation for 72 h significantly

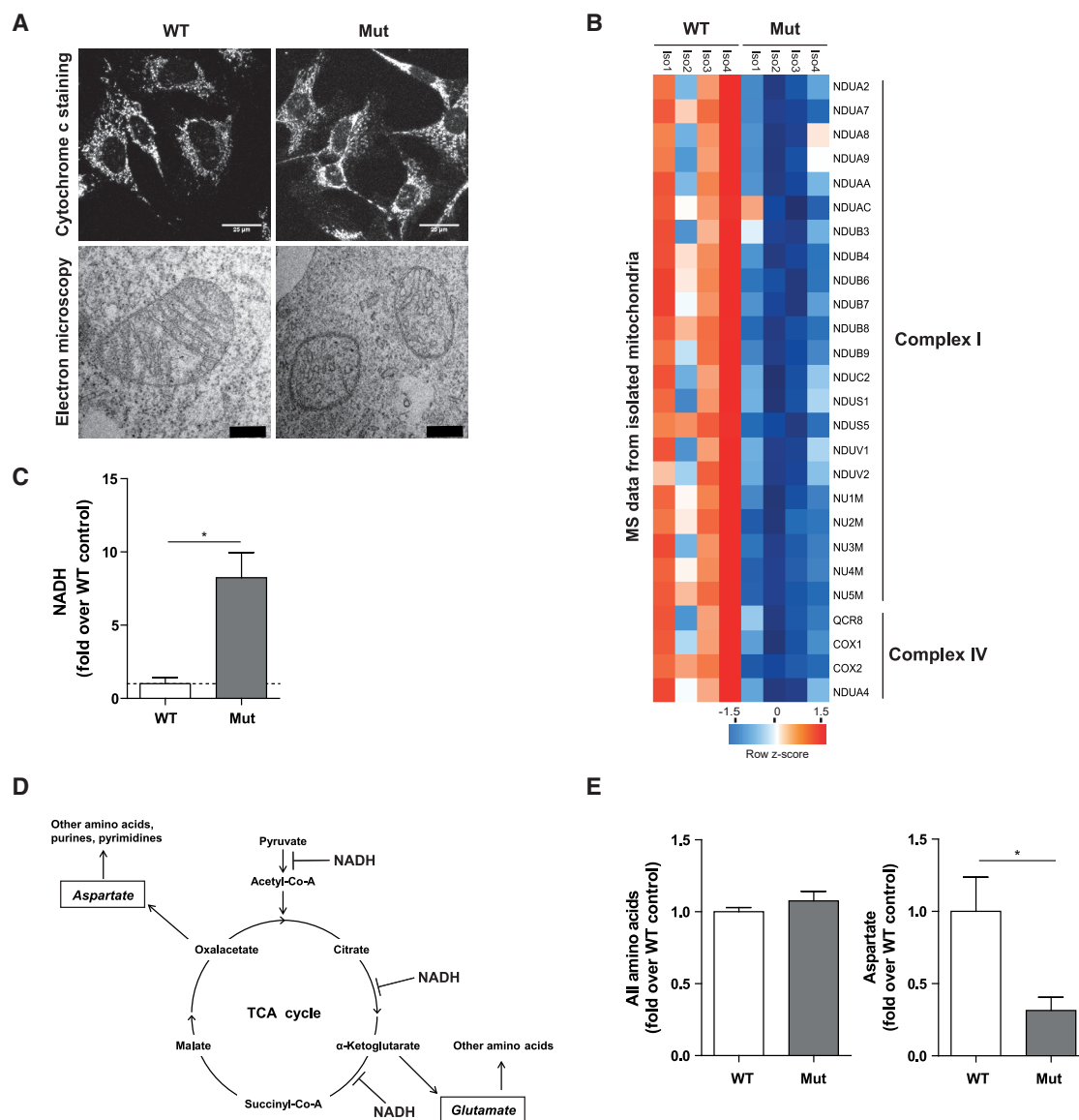


Figure 2. Respiratory Chain Dysfunction Results in Aspartate Deficiency

(A) Representative images of the mitochondrial network in WT (n = 3) and Mut (n = 4) cells visualized by staining with anti-cytochrome c antibody (upper panel). Scale bar: 25 μ m. Lower panel shows representative electron microscopy images of mitochondria in a single WT and Mut cell line. Scale bar: 1 μ m.

(B) Heatmap representing Z scored relative protein mass-spectrometric intensities of significantly regulated respiratory chain complex subunits of mitochondria isolated from one Mut (four technical replicates) and one WT (four technical replicates) cell line.

(C) NADH levels in WT (n = 3) and Mut (n = 4) cells. Bar graphs show mean \pm SEM relative to WT cells. Statistical test: Student's unpaired t test.

(D) Scheme of the TCA cycle emphasizing its role in amino acid synthesis and its inhibition by increased NADH levels. The amino acids aspartate and glutamate are directly synthesized from TCA cycle intermediates and serve as precursors for the synthesis of other amino acids and purines and pyrimidines.

(E) Levels of all amino acids were determined by mass-spectrometry-based targeted metabolomics in WT (n = 3) and Mut (n = 4) cells. Six replicates were measured for each cell line and the respective values were normalized to the cell number of each cell line. Bar graphs show mean \pm SEM relative to WT controls for all amino acids together and a single quantification for aspartate. Significance was determined using Student's unpaired t test.

See also Figure S2.

increased the activity of the proteasome in mutator cells (Figure 3A). Aspartate treatment specifically activated the assembly and activity of mainly double-capped 26S proteasomes (Figure 3B). Proteasome activation was first evident after 24 h of aspartate treatment (Figure S3A). Aspartate did not affect pro-

teasome function in WT cells (Figure S3B). Pyruvate—which serves as an electron acceptor at conditions of redox imbalance (Sullivan et al., 2015)—also clearly increased single- and double-capped 26S proteasome assembly (Figure 3C), but did not affect proteasome activity in WT cells (Figure S3C).

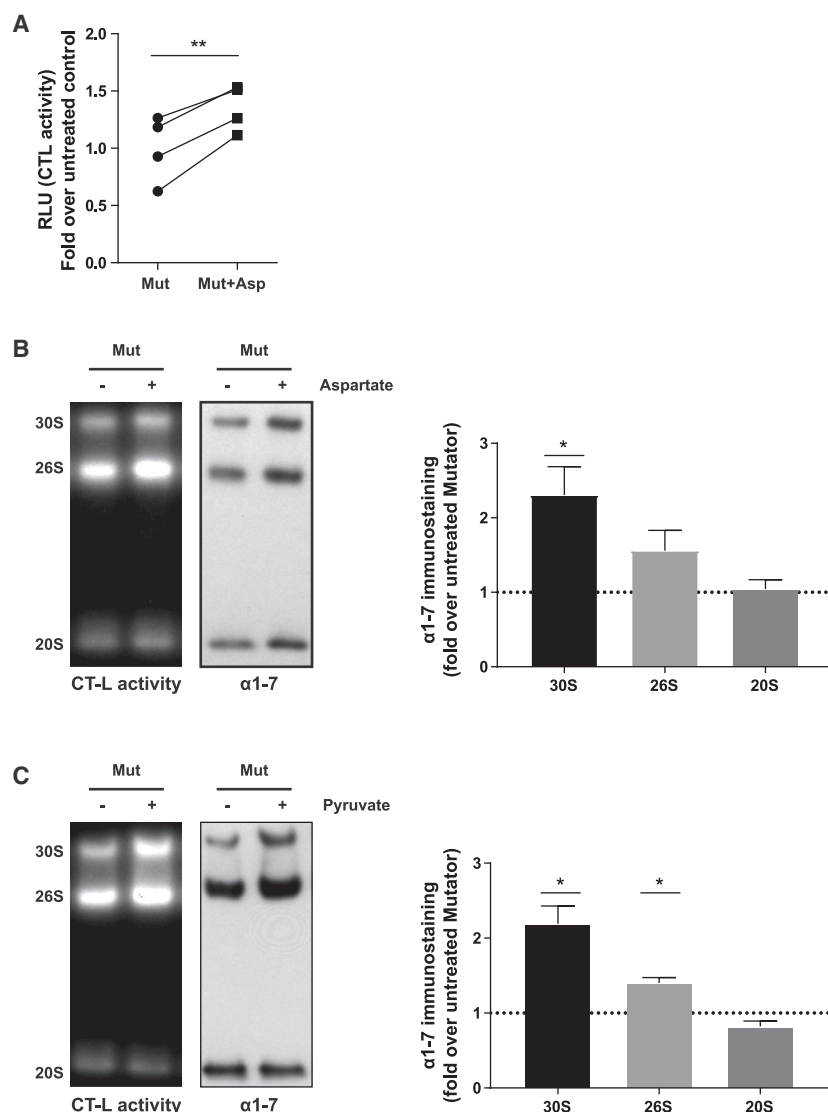


Figure 3. Supplementation of Aspartate Activates 26S Proteasome Activity

(A) Proteasome activity in total cell extracts of Mut cells ($n = 4$) treated with 10-mM aspartate for 72 h as determined by cleavage of luminogenic substrates specific for the CT-L activity. Graph shows values of aspartate-treated cells that were normalized to the mean of untreated controls. Statistical test: Student's paired t test.

(B) Representative native gel analysis of active proteasome complexes in cell lysates from Mut cells treated with 10-mM aspartate for 72 h. CT-L substrate overlay assay and immunoblotting for 20S α 1–7 subunits is shown. The resolution of double-capped (30S) and single-capped 26S proteasomes (26S) is indicated together with the 20S proteasome complexes (20S). Bar graphs represent mean \pm SEM of immunostaining signal relative to the respective untreated Mut cells ($n = 4$ cell lines). Significance was determined using one sample Student's t test.

(C) Representative native gel analysis of active proteasome complexes in cell lysates from Mut cells treated with 1-mM pyruvate for 72 h. CT-L substrate overlay assay and immunoblotting for 20S α 1–7 subunits is shown. Bar graphs represent mean \pm SEM relative to the respective untreated Mut cells ($n = 3$ cell lines). Significance was determined using one sample Student's t test.

See also Figure S3.

Aspartate Supplementation Induces Assembly of 26S Proteasomes

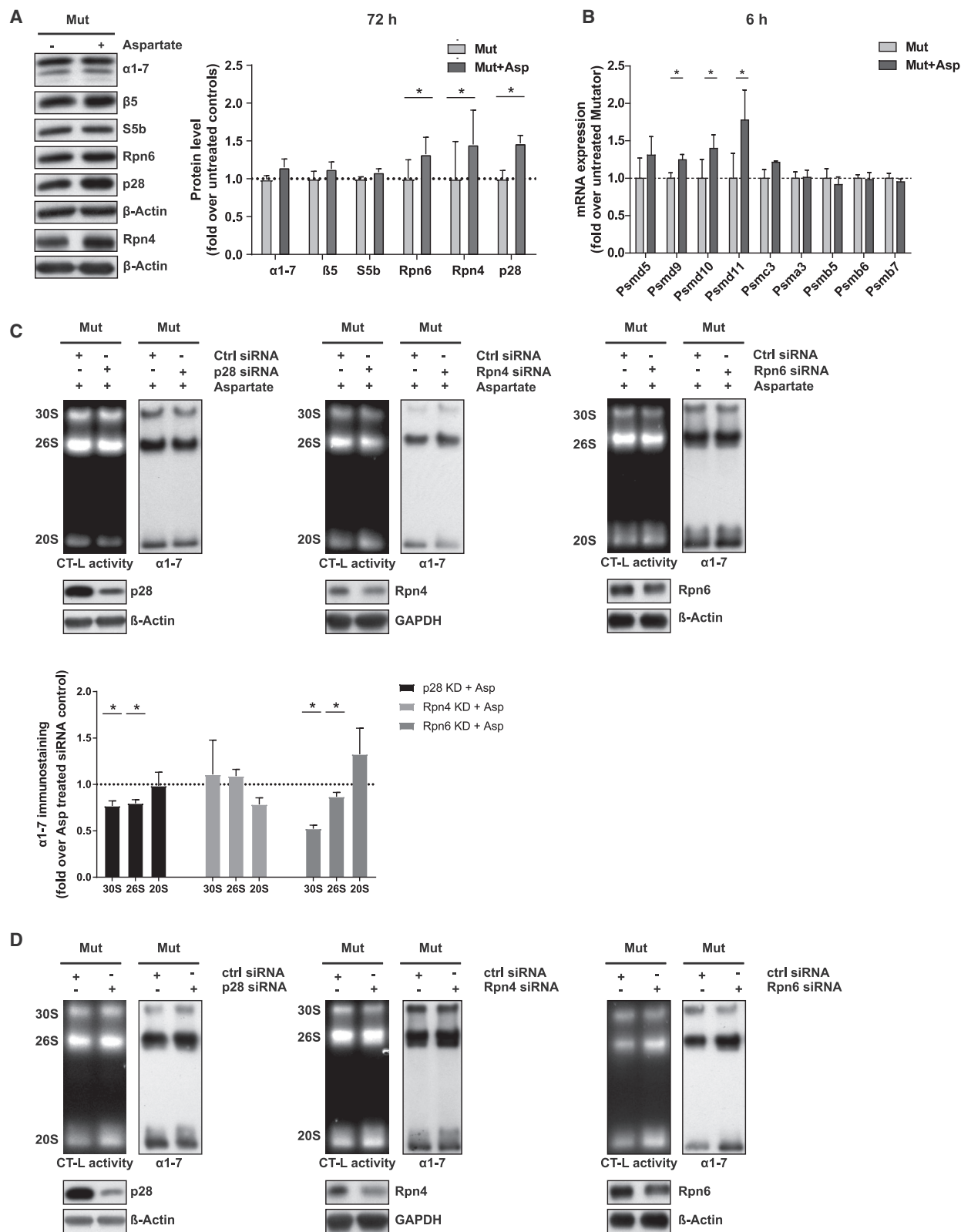
To investigate the underlying mechanism for metabolic activation of 26S proteasome assembly, we first analyzed whether aspartate supplementation affects expression of proteasome subunits. Overall expression of proteasomal subunits was not altered as determined by western blotting for 20S α and the β 5 subunits (Figure 4A). In contrast, we noticed specific aspartate-mediated upregulation of several 26S proteasome assembly factors, i. e. the assembly chaperones Rpn4 and p28 and the 19S subunit Rpn6, while S5b was not regulated by aspartate (Figure 4A). Aspartate induced RNA expression of the respective assembly factors (Psm9 for Rpn4, Psm10 for p28, and Psm11 for Rpn6) already after 6 h (Figure 4B). Silencing of p28 but not Rpn4 counteracted assembly of 26S proteasomes upon supplementation with aspartate in mutator cells as demonstrated by native gel and immunoblotting analysis (Figure 4C).

Depletion of p28 in the absence of aspartate treatment did not alter 26S proteasome assembly (Figure 4D). Partial silencing of Rpn6 similarly neutralized aspartate-induced 26S assembly and activation (Figures 4, C and D). While Rpn4 and p28 act as 19S regulatory particle assembly-chaperones (RACs; Kaneo et al., 2009), Rpn6 is an integral part of the 19S regulator and serves as a molecular clamp that stabilizes the interaction with the 20S (Pathare et al., 2012). Accordingly, full depletion of Rpn6 is detrimental for the cell, but an only minor increase in its expression

level promotes assembly of 26S proteasome complexes (Semren et al., 2015; Vilchez et al., 2012), whereas partial depletion counteracts 26S assembly (Semren et al., 2015). Of note, the same assembly factors were downregulated in mutator compared to WT cells, while S5b—which is also known to inhibit 26S assembly (Levin et al., 2018; Shim et al., 2012)—was upregulated (Figure S4). Our data thus demonstrate that metabolic regulation of 26S assembly factors is a key determinant in regulating the adaptive assembly of 26S proteasome complexes at conditions of mitochondrial dysfunction.

Aspartate Activates Multiple Cellular Signaling Pathways, Including mTOR Signaling

We further dissected the mechanism by which aspartate activates 26S proteasome assembly in an unbiased phosphoproteome screen. Mutator cells were treated for 4 h with or without aspartate. Phosphorylated peptides were enriched and identified



(legend on next page)

by mass spectrometry analysis according to a recently published protocol of the Mann lab (Humphrey et al., 2018). We identified almost 10,000 phosphorylation sites with 233 phosphosites being significantly regulated by aspartate treatment. These mapped to 177 proteins (Table S6). About half of them were increased in abundance upon aspartate treatment (Figure S5A). We identified numerous key regulators of the cell cycle, DNA replication, cytoskeleton, ribosome, transcription, and growth factor signaling pathways (Table S5). Proteasome subunits were not differentially phosphorylated by aspartate (Figure S5B). Inspection of the kinase consensus motifs of the phosphorylated peptides identified several kinases that were activated by aspartate (Figure 5A; Table S7). Among these were several cell-cycle-related kinases such as CDK1, Aurora A, GSK3, ERK1, ERK2, and CDK5 besides other growth-factor, cell-cycle, and metabolic-signaling kinases (Figure 5A). This observation is well in line with the essential function of aspartate for proliferation (Birsoy et al., 2015; Sullivan et al., 2015) and aspartate-mediated induction of proliferation in mutator cells (Figure S5C). Other most predominantly activated kinases were the p70 ribosomal S6 kinase and MAPKAP1, MAPKAP2, and AKT kinases, which are all involved in the activation of protein synthesis via the mTOR pathway (Saxton and Sabatini, 2017). Activation of the mTOR pathway by aspartate was confirmed by enhanced phosphorylation of the p70 S6 kinase and the S6 ribosomal protein in western blots (Figure 5B). In accordance with the activation of mTOR signaling, aspartate treatment for 72 h increased protein synthesis in mutator cells (Figure 5C). Very similar mTOR signaling and protein synthesis were found to be diminished in mutator compared to WT cells (Figures S5D and S5E). Low doses of rapamycin (0.5 nM) effectively counteracted aspartate-induced activation of mTORC1 signaling (Figure S5F). These data demonstrate a previously unrecognized regulation of protein synthesis by aspartate via the mTORC1 complex. Importantly, mTOR inhibition by rapamycin effectively prevented aspartate-induced upregulation of the proteasome assembly factors p28 and Rpn6 (Figure 5D) and activation of 26S proteasome assembly (Figure 5E). Rapamycin did not affect, however, proteasome activity and assembly in untreated mutator cells (Figure S5G). Similar effects were observed upon silencing of raptor, a specific component of the mTORC1 complex (Saxton and Sabatini, 2017; Figures S5H and S5I). These data demonstrate that aspartate activates the mTORC1 pathway, which—by a currently unknown pathway—induces the transcrip-

tional activation of specific proteasome assembly factors to promote assembly of 26S proteasome complexes.

Defective Complex I Function Drives Metabolic Adaptation of the Proteasome in Human Cells

Our data obtained with the mutator cells strongly indicate that the defective electron transfer at complex I is the major driver for the observed metabolic regulation of 26S proteasome function. We thus tested whether the proteasome is metabolically regulated in cells with defined genetic complex I dysfunction. Skin fibroblasts were obtained from a patient with a hereditary mutation in the ND5 subunit of respiratory complex I (Kremer et al., 2017). These cells showed significantly diminished proteasome activity (Figure 6A) that we could attribute to reduced assembly and activity of 26S proteasome complexes (Figure 6B). Supplementation with aspartate activated assembly and activity of 26S proteasome complexes in ND5 mutant cells in a manner very similar to our results obtained with the mutator cells (Figure 6C). In a second approach, we applied pharmacological inhibition of complex I. For that, we used metformin—a well-known anti-diabetic drug that inhibits complex I activity in the absence of ROS production (Sullivan et al., 2015). Of note, metformin treatment of primary healthy human skin fibroblasts for 72 h significantly inhibited the assembly and activity of 26S proteasome complexes. This effect was fully restored by supplementation of either aspartate or pyruvate (Figure 6D). Similarly, metformin effectively inhibited 26S proteasome assembly in primary human lung fibroblasts, which was alleviated by treatment with aspartate or pyruvate (Figure 6E). Very similar results were obtained with WT MEFs (Figure S6).

Our results thus reveal a reversible adjustment of 26S proteasome activity by aspartate or pyruvate under conditions of respiratory complex I dysfunction. They unravel a previous unknown cellular consequence of respiratory chain dysfunction for proteasomal protein degradation. Moreover, our findings suggest that metabolic inhibition of proteasome function can be alleviated by treatment with aspartate or pyruvate, which may have therapeutic implications.

Respiratory Chain Dysfunction Confers Resistance to the Proteasome Inhibitor Bortezomib

To investigate the physiological relevance of reduced 26S proteasome activity and assembly in cells with respiratory

Figure 4. Aspartate Supplementation Induces Assembly of 26S Proteasomes

(A) Representative western blot analysis of 20S (α 1–7, β 5) and 19S (Rpn6, Rpn4, p28, S5b) subunit expression in Mut cells treated with 10-mM aspartate for 72 h. β -actin was used as a loading control. Densitometric analysis shows mean \pm SEM from four Mut cell lines. Significance was determined using Student's paired t test. (B) qRT-PCR analysis of proteasome subunit mRNA expression in Mut (n = 3) cells after 6 h of aspartate treatment. Data represent mean \pm SEM relative to untreated controls. Significance was determined using Student's paired t test. (C) Representative native gel analysis of active proteasome complexes and quantification thereof in cell lysates from one Mut cell line upon p28 (n = 4 independent experiments), Rpn4 (n = 3 independent experiments), and Rpn6 (n = 5 independent experiments) silencing and aspartate treatment for 72 h with CT-L substrate overlay assay and immunoblotting for 20S α 1–7. The resolution of double-capped (30S) and single-capped 26S proteasomes (26S) is indicated together with the 20S proteasome complexes (20S). Control cells were transfected with two different scrambled control small interfering RNAs (siRNAs). Densitometric analysis shows mean \pm SEM of fold change over control from the respective replicate. Significance was determined using the one sample Student's t test. Knockdown was confirmed via immunostaining for p28, Rpn4, and Rpn6. Only partial knockdown of Rpn6 was used to prevent cellular stress. (D) Representative native gel analysis of active proteasome complexes in cell lysates from one Mut cell line upon p28, Rpn4, and Rpn6 silencing for 72 h with CT-L substrate overlay assay, immunoblotting for 20S α 1–7 and quantification thereof. Control cells were transfected with a combination of two different control siRNAs. See also Figure S4.

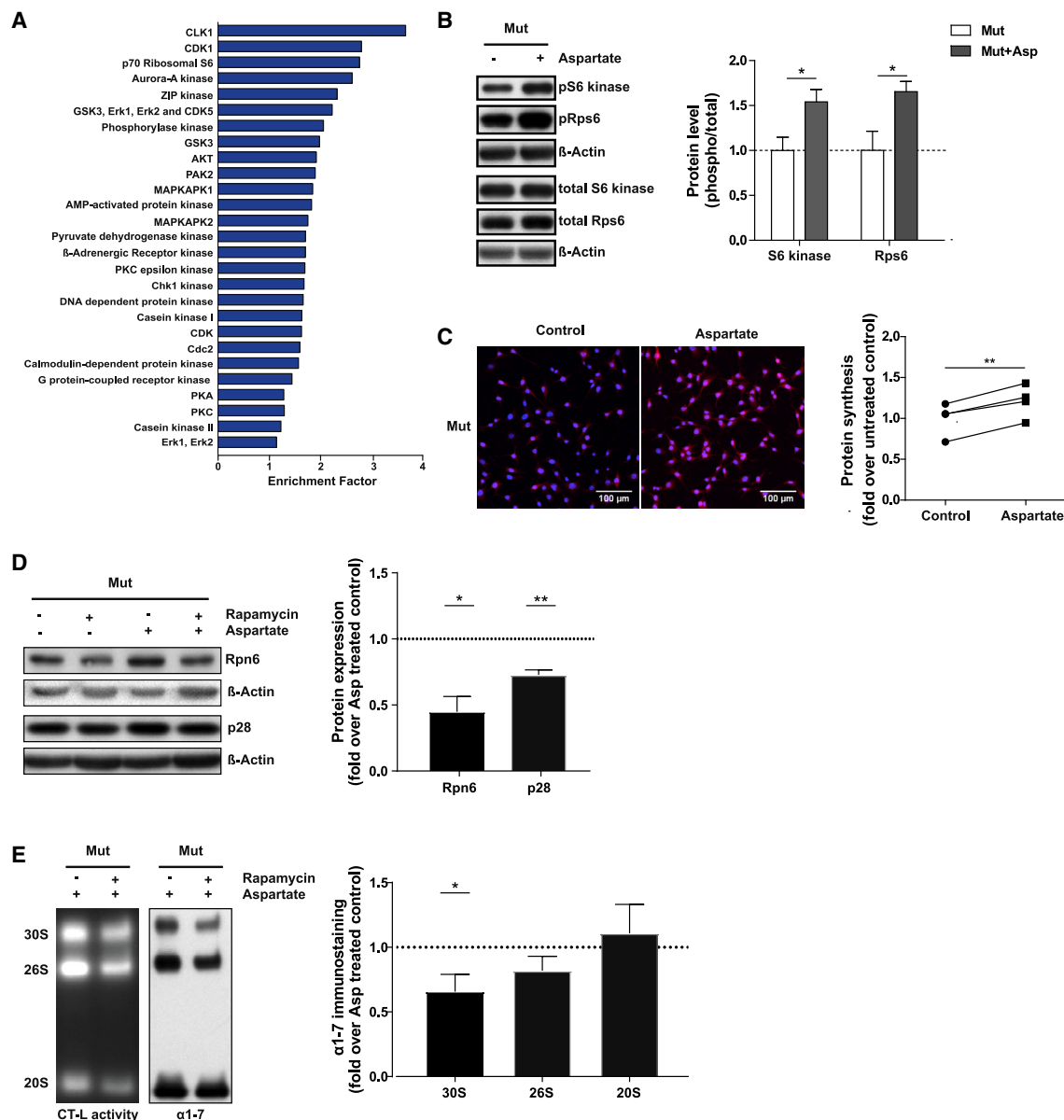


Figure 5. Aspartate Activates Multiple Cellular Signaling Pathways, Including mTOR Signaling

(A) Enrichment analysis of phosphoproteomics data for kinases predicted to be activated upon aspartate treatment using Fisher exact test (FDR > 0.02).

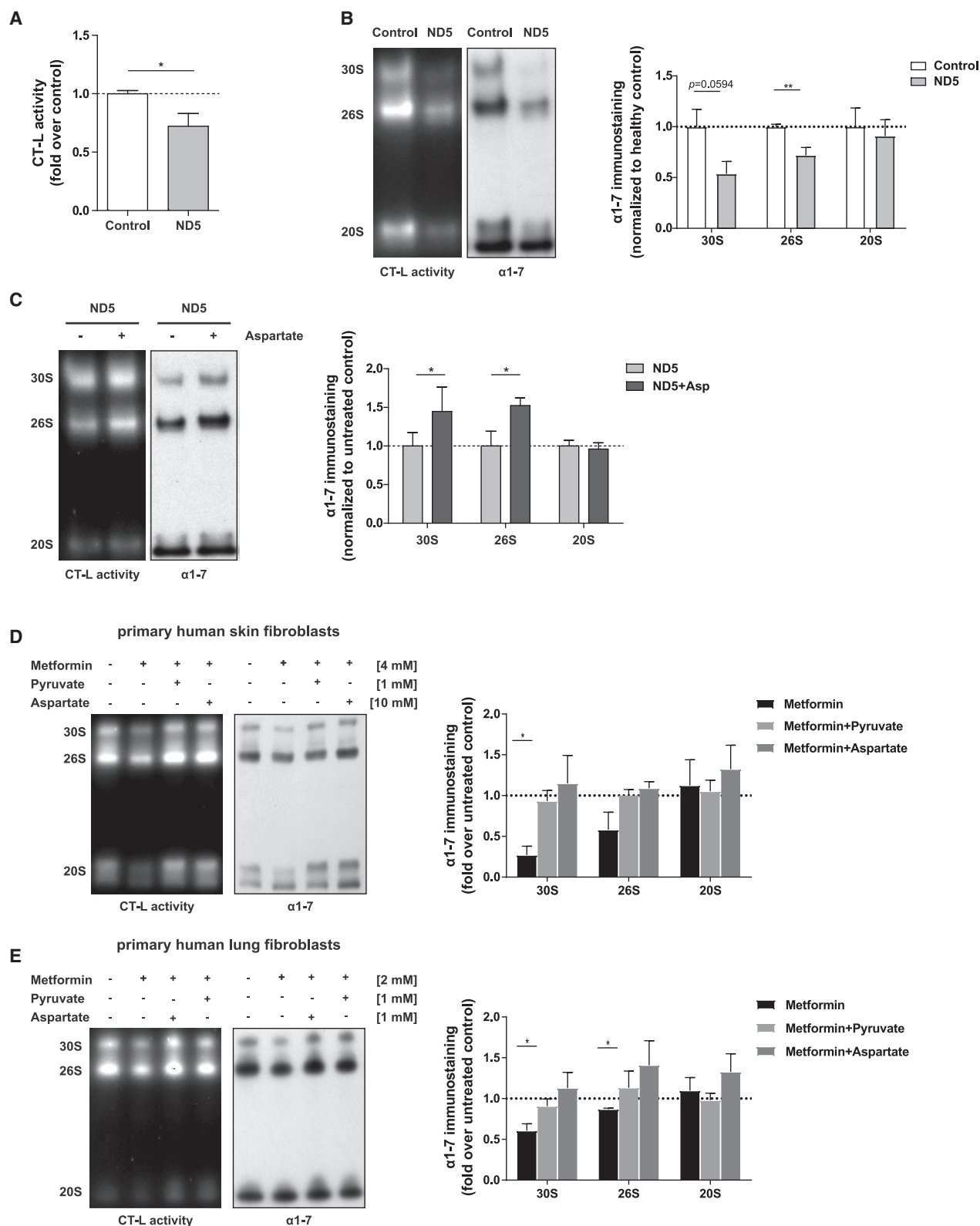
(B) Analysis of mTORC1 signaling after treatment with 10-mM aspartate for 48 h in Mut cells. Representative western blots of total and phosphorylated levels of p70 S6 kinase and S6 ribosomal protein (Rps6). β-actin served as a loading control. Bar graphs show β-actin-normalized phosphoprotein levels related to β-actin-normalized total levels of the respective protein in Mut cell lines (n = 4; mean ± SEM). Significance was determined using Student's unpaired t test.

(C) Cellular protein synthesis rate was determined using the puromycin analog OPP (O-propargyl-puromycin). Representative fluorescence images of nascent protein synthesis (red signal) and nucleic staining (blue signal) after supplementation of Mut cells (n = 4) with 10-mM aspartate for 48 h are shown. Mut controls were cultured for 48 h in normal medium containing no aspartate. Quantification of protein synthesis (mean fluorescent intensity [MFI] of red signal) reveals differences in protein synthesis between the individual Mut cell lines with and without aspartate supplementation. Scale bar: 100 μm. Statistical test: Student's paired t test.

(D) Analysis of 26S proteasome assembly factor expression upon treatment with 0.5-nM rapamycin and 10-mM aspartate for 72 h in one Mut cell line. β-actin was used as a loading control. Bar graphs show fold change of aspartate and rapamycin co-treatment over aspartate-treated control. Significance was determined using a one-sample Student's t test.

(E) Representative native gel analysis of active proteasome complexes and quantification thereof in cell lysates from one Mut cell line upon treatment with 0.5-nM rapamycin and 10-mM aspartate for 72 h with CT-L substrate overlay assay and immunoblotting for 20S α1-7. Densitometric analysis shows mean ± SEM of fold change of aspartate and rapamycin co-treatment over aspartate-treated control from three independent experiments. Significance was determined using a one-sample Student's t test.

See also Figure S5.



(legend on next page)

dysfunction, we tested the cellular response toward proteasome inhibition in mutator cells. WT and mutator cells were treated with increasing doses of the USA Food and Drug Administration (FDA)-approved proteasome inhibitor bortezomib, and cell viability was monitored. Of note, cells with mitochondrial dysfunction showed higher resistance toward bortezomib-induced cell death (Figures 7A and S7A). Annexin V/ propidium iodide (PI) staining confirmed reduced apoptotic cell death in mutator compared to WT cells with toxic doses of bortezomib (25 nM; Figures S7B and S7C). This protective effect was specific for proteasome inhibition and not observed when cells were exposed to increasing concentrations of H_2O_2 (Figure S7D). We next analyzed if the resistance toward bortezomib in mutator MEFs can be reversed by supplementation of pyruvate. Supplementation of mutator cells with 1-mM pyruvate for 24 h followed by treatment with increasing concentrations of bortezomib restored sensitivity toward proteasome inhibition, as shown by significantly reduced cell viability compared to non-pyruvate-treated mutator cells (Figure 7B). To analyze whether bortezomib resistance can be induced by respiratory complex I dysfunction, WT cells were pretreated with 5-mM metformin for 24 h and subsequently treated with increasing doses of bortezomib. Notably, metformin pretreatment significantly increased resistance toward bortezomib (Figure 7C). This effect was fully reversible when cells were pretreated with a combination of metformin and pyruvate (Figure 7D). From these data, we conclude that mitochondrial dysfunction contributes to the resistance toward proteasome inhibition possibly due to reduced activity of the 26S proteasome, as recently shown for bortezomib-resistant tumor cells (Acosta-Alvear et al., 2015; Tsvetkov et al., 2015, 2017).

DISCUSSION

In this study, we demonstrate that respiratory complex I dysfunction inhibits the activity of the ubiquitin-proteasome system by metabolic reprogramming. Impairment of 26S assembly is observed upon chronic impairment of mitochondrial function such as in mutator cells and ND5 mutant patient cells, and also upon acute inhibition of complex I by metformin in the absence

of oxidative stress. Importantly, inhibition can be fully reversed by supplementation of aspartate or pyruvate, thus demonstrating adaptive metabolic fine-tuning of 26S proteasome function, which may have therapeutic implications.

It is well established that the 26S proteasome can be upregulated via concerted transcriptional induction of proteasomal gene expression under conditions of increased protein hydrolysis, protein stress, cell growth, and p53 signaling (Meiners et al., 2003; Sha and Goldberg, 2014; Walerych et al., 2016; Zhang et al., 2014). However, transcriptional regulation of proteasome function is not suitable for rapid and reversible adaptation to cellular needs (Meiners et al., 2014; Rousseau and Bertolotti, 2018). Rapid adjustment of 26S proteasome activity to growth signals can be achieved by post-translational modifications of 19S or 20S subunits as, e.g., elegantly shown for the 19S subunits Rpt3 (Guo et al., 2016; VerPlank and Goldberg, 2017) and Rpn1 (Liu et al., 2020). In addition, assembly chaperones regulate the formation of 26S proteasome complexes from the 20S catalytic core and 19S regulatory particles, thus allowing timely adjustment of 26S proteasome activity to cellular demands (Kane et al., 2009; Rousseau and Bertolotti, 2018). The RACs S5b, Rpn4, and p28 were found to be rapidly induced via extracellular regulated kinase (ERK) 5 by inhibition of the mTOR pathway (Rousseau and Bertolotti, 2016). Similarly, phosphorylation of the constitutive 19S subunit Rpn6 by protein kinase A promoted assembly of 26S complexes upon acute mTOR inhibition (Lokireddy et al., 2015; VerPlank et al., 2019). Such activation of 26S proteasome function under conditions of mTOR inhibition parallels that of autophagy induction to ensure cellular amino acids supply (Saxton and Sabatini, 2017). In contrast to these data, the Manning lab demonstrated concerted activation of proteasome expression upon sustained inhibition of the mTOR signaling pathway (Zhang et al., 2014). This effect involved concerted transcriptional upregulation of proteasomal gene expression via the transcription factor Nrf1, a well-known regulator of proteasomal gene expression (Sha and Goldberg, 2014; Steffen et al., 2010). We here demonstrate a different type of regulation of proteasome assembly via the mTORC1 complex: activation of the mTOR pathway by aspartate induced

Figure 6. Defective Complex I Function Drives Metabolic Adaptation of the Proteasome in Human Cells

(A) Proteasome activity was measured in total cell extracts of ND5 mutant human fibroblasts and healthy controls in five different replicates from different cell passages using a luminogenic substrate specific for the CT-L active site of the proteasome. Data represent mean \pm SEM relative to controls. Statistical test: Student's unpaired t test.

(B) Representative native gel analysis of active proteasome complexes in native cell lysates from human skin fibroblasts (healthy control and ND5 mutant) and quantification thereof with CT-L substrate overlay assay and immunoblotting for 20S α 1–7. The resolution of double-capped (30S) and single-capped 26S proteasomes (26S) is indicated together with the 20S proteasome complexes (20S). Four independent experiments were performed. Bar graphs show mean \pm SEM relative to healthy control. Significance was determined using Student's unpaired t test comparing healthy control versus ND5 mutant cells.

(C) ND5 mutant patient fibroblasts were treated with 10-mM aspartate for 48 h in six independent experiments. Activity and assembly of proteasome complexes was analyzed by native gel electrophoresis with CT-L substrate overlay assay and immunoblotting for 20S α 1–7 subunits. Densitometry shows mean \pm SEM values of aspartate-treated relative to untreated fibroblasts. Significance was determined using Student's unpaired t test.

(D) Representative native gel analysis of active proteasome complexes in cell lysates from healthy primary human skin fibroblasts co-treated with 10-mM aspartate or 1-mM pyruvate together with 4-mM metformin for 72 h. CT-L substrate overlay assay and immunoblotting for 20S α 1–7 subunits is shown. Bar graphs represent mean \pm SEM relative to respective untreated skin fibroblasts (n = 4 independent experiments). Significance was determined using a one-sample Student's t test.

(E) Representative native gel analysis of active proteasome complexes in cell lysates from healthy primary human lung fibroblasts cotreated with 1-mM aspartate or 1-mM pyruvate together with 2-mM metformin for 72 h. CT-L substrate overlay assay and immunoblotting for 20S α 1–7 subunits is shown. Bar graphs represent mean \pm SEM relative to respective untreated lung fibroblasts (n = 4 independent experiments). Significance was determined using a one-sample Student's t test.

See also Figure S6.

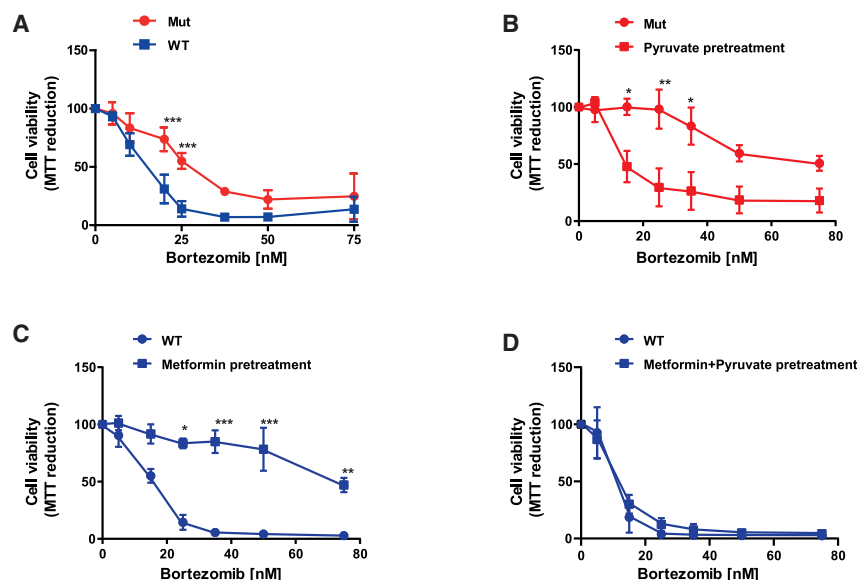


Figure 7. Respiratory Chain Dysfunction Confers Resistance to the Proteasome Inhibitor Bortezomib

(A) MTT cellular viability assay of WT (n = 3) and Mut (n = 4) MEFs treated with increasing doses of the proteasome inhibitor bortezomib for 48 h. (B) MTT cellular viability assay of three different Mut MEF cell lines pretreated with 1-mM pyruvate for 24 h followed by treatment with increasing doses of the proteasome inhibitor bortezomib for 48 h. (C) MTT cellular viability assay of three different WT MEF cell lines pretreated with 5-mM metformin for 24 h followed by treatment with increasing doses of the proteasome inhibitor bortezomib for 48 h. (D) MTT cellular viability assay of three different WT MEF cell lines pretreated with 5-mM metformin and 1-mM pyruvate for 24 h followed by treatment with increasing doses of the proteasome inhibitor bortezomib for 48 h. Values were normalized to the solvent-treated control (0-nM bortezomib) and are displayed as mean \pm SEM. Significance was determined using two-way ANOVA with a Bonferroni multiple comparison test. *p < 0.05, **p < 0.01, ***p < 0.001. See also Figure S7.

transcriptional upregulation of only 26S assembly factors, i.e., Rpn4, p28, and Rpn6, but did not activate gene expression of other 20S or other 19S subunits. This selective transcriptional activation makes it highly unlikely that Nrf1 is involved in this process (Zhang et al., 2014). Our phosphoproteomics analysis also excluded altered phosphorylation of Rpn6 and regulation of ERK5 to be involved in this process. Importantly, the two assembly factors p28 and Rpn6 were required for the induction of 26S proteasome assembly by supplementation of aspartate. We also demonstrate that this regulation is reversible as aspartate or pyruvate supplementation was sufficient to restore defective 26S proteasome assembly upon metformin treatment. Nucleoside addition, however, did not rescue proteasome assembly. These data suggest that nucleotide deficiency is not rate limiting but rather the apparent lack of electron acceptors. The adaptive nature of this regulation is also supported by the fact that the mutator cells do not display any signs of protein stress such as accumulation of polyubiquitinated proteins or folding chaperones at conditions of reduced 26S proteasome activity. Of note, reversible adjustment of 26S proteasome assembly was also evident in other cell types, i.e., MEFs and primary human skin or lung fibroblasts, indicating a robust and conserved mechanism of metabolic fine-tuning of proteasome function. These findings add an important aspect of proteasome regulation and fit to the emerging concepts of fine-tuning of proteasome activity and also ribosome function according to cellular needs (Emmott et al., 2019; Meiners et al., 2014; Rousseau and Bertolotti, 2018; Wang et al., 2020).

The specific nature of how aspartate activates the mTORC1 complex is currently unknown. Our phosphoproteomic analysis revealed that aspartate activated the p70 ribosomal S6 kinase, MAPKAP1, MAPKAP2, and AKT kinases after 4 h of aspartate treatment, raising the possibility of direct aspartate sensing by the mTORC1 complex. However, as kinases also involved in growth-factor, cell-cycle, and metabolic signaling were acti-

vated, we cannot exclude other regulatory mechanisms such as, for example, tRNA uncharging, nucleotide limitation, AMP-activated protein kinase (AMPK) pathway activation, or an altered NAD/NADH ratio to be involved in aspartate-mediated regulation of the mTOR pathway.

Our findings establish a fundamental and previously unrecognized interaction between mitochondrial function and the ubiquitin-proteasome system. Specifically, impaired activity of respiratory complex I and subsequent reprogramming of the TCA cycle with deficiency of aspartate and electron acceptors results in reduced 26S proteasome activity. This interaction is of significant relevance to aging and disease: both aging and diseases of proteostasis imbalance such as neurodegenerative and cardiac diseases are characterized by respiratory chain dysfunction and impaired proteasome activity (Ciechanover and Brundin, 2003; Drews and Taegtmeier, 2014; Karamanlidis et al., 2013; Kauppila et al., 2017; López-Otín et al., 2013; Schapira et al., 1989). It is tempting to speculate that glycolytic reprogramming of tumor cells might contribute to diminished protein synthesis and 26S proteasome activity to confer resistance toward proteasome inhibitor treatment. Impaired 26S activity has previously been established as a prominent feature of proteasome inhibitor resistance (Acosta-Alvear et al., 2015; Tsvetkov et al., 2015, 2017). In accordance, the mutator cells with their reduced protein synthesis and 26S proteasome function were more resistant toward bortezomib treatment. Pyruvate supplementation, which activates 26S proteasome activity, restored sensitivity to bortezomib treatment. Similarly, metformin treatment reversibly induced resistance toward bortezomib in respiration-deficient cells, which was fully reversed by pyruvate co-treatment. These data strongly support the recent findings by Tsvetkov et al. (2017, 2019) that proteasome and mitochondrial function are closely linked with proteasome inhibitor resistance. Activating 26S proteasome assembly and activity by supplementation of aspartate or pyruvate might provide a therapeutic concept to

counteract imbalanced proteostasis in disease and upon drug treatment.

STAR★METHODS

Detailed methods are provided in the online version of this paper and include the following:

- **KEY RESOURCES TABLE**
- **RESOURCE AVAILABILITY**
 - Lead Contact
 - Materials Availability
 - Data and Code Availability
- **EXPERIMENTAL MODEL AND SUBJECT DETAILS**
 - Cell culture
- **METHOD DETAILS**
 - Protein extraction
 - Proteasome activity assays
 - Western blot analysis
 - Native gel analysis
 - Primer sequences for qRT-PCR
 - Quantitative real-time RT-PCR
 - Measurement of ATP levels
 - Analysis of reactive oxygen species (ROS) in cells
 - Cellular oxygen consumption
 - Mitochondrial cytochrome c staining
 - Isolation of mitochondria
 - Electron microscopy
 - Measurement of cellular NADH levels
 - Metabolomic analysis
 - Aspartate and pyruvate supplementation
 - Metformin treatment
 - Lysate preparation for phosphoproteome analysis (Humphrey et al., 2018)
 - Phosphopeptide enrichment
 - StageTip desalting of phosphopeptides
 - Bioinformatic analysis of phosphoproteomics data
 - Filter-aided sample preparation for proteomic analysis
 - Proteomic analysis
 - Progenesis Q1 for label-free quantification
 - Mitominer analysis
 - Bioinformatic analysis of proteomics data
 - Cell proliferation assay
 - Protein synthesis assay (WT versus mutator MEFs)
 - Protein synthesis assay (aspartate treatment of mutator MEFs)
 - siRNA mediated mRNA silencing
 - Rapamycin and aspartate cotreatment of mutator cells
 - Bulk mRNA sequencing
 - Cotreatment of bortezomib and pyruvate/metformin
 - Cell viability assay (MTT)
 - Live/dead staining with annexin V/PI
- **QUANTIFICATION AND STATISTICAL ANALYSIS**

SUPPLEMENTAL INFORMATION

Supplemental Information can be found online at <https://doi.org/10.1016/j.celrep.2020.108059>.

ACKNOWLEDGMENTS

T.M. and K.B. were supported by the CPC/Helmholtz Graduate School program “Lung Biology and Disease.” F.P. was supported by the Munich Center for Systems Neurology (SyNergy EXC 2145/ID 390857198) and The Bert L & N Kuggie Vallee Foundation. H.P. was supported by German Federal Ministry of Education through a grant to the German Network for Mitochondrial Disorders (01GM1906) and the E-Rare project GENOMIT (01GM1603 and 01GM1207). We are grateful for the support by Jennifer Wettmarshausen, and for the excellent technical assistance of Carola Eberhagen. We are also very grateful for the support in the RNA sequencing data upload by Meshal Ansari.

AUTHOR CONTRIBUTIONS

T.M., K.B., S.S., C.L., C.S., L.F.M., A.S.Y., X.W., C.P., L.K., C.v.T., and B.P. performed the experiments; T.M., K.B., S.S., C.P., C.H.M., H.B.S., L.F.M., J.A., L.K., H.P., F.P., C.v.T., S.M.H., H.Z., and S.M. analyzed and discussed the data; H.P., A.K., and A.T. provided cells and animals; T.M., C.P., S.S., and C.H.M. prepared the figures; and T.M., S.S., H.Z., and S.M. wrote the manuscript.

DECLARATION OF INTERESTS

The authors declare no competing interests.

Received: April 8, 2020

Revised: June 18, 2020

Accepted: July 31, 2020

Published August 25, 2020

REFERENCES

- Acosta-Alvarez, D., Cho, M.Y., Wild, T., Buchholz, T.J., Lerner, A.G., Simakova, O., Hahn, J., Korde, N., Landgren, O., Maric, I., et al. (2015). Paradoxical resistance of multiple myeloma to proteasome inhibitors by decreased levels of 19S proteasomal subunits. *eLife* 4, e08153.
- Ahn, C.S., and Metallo, C.M. (2015). Mitochondria as biosynthetic factories for cancer proliferation. *Cancer Metab.* 3, 1.
- Anders, S., Pyl, P.T., and Huber, W. (2015). HTSeq—a Python framework to work with high-throughput sequencing data. *Bioinformatics* 31, 166–169.
- Bard, J.A.M., Goodall, E.A., Greene, E.R., Jonsson, E., Dong, K.C., and Martin, A. (2018). Structure and function of the 26S proteasome. *Annu. Rev. Biochem.* 87, 697–724.
- Birsoy, K., Wang, T., Chen, W.W.W., Freinkman, E., Abu-Remaileh, M., and Sabatini, D.M.M. (2015). An essential role of the mitochondrial electron transport chain in cell proliferation is to enable aspartate synthesis. *Cell* 162, 540–551.
- Calvo, S.E., Clauser, K.R., and Mootha, V.K. (2016). MitoCarta2.0: an updated inventory of mammalian mitochondrial proteins. *Nucleic Acids Res.* 44 (D1), D1251–D1257.
- Chandel, N.S. (2015a). Navigating Metabolism. (Cold Spring Harbor Laboratory Press).
- Chandel, N.S.S. (2015b). Evolution of mitochondria as signaling organelles. *Cell Metab.* 22, 204–206.
- Chou, A.P., Li, S., Fitzmaurice, A.G., and Bronstein, J.M. (2010). Mechanisms of rotenone-induced proteasome inhibition. *Neurotoxicology* 31, 367–372.
- Ciechanover, A. (2015). The unravelling of the ubiquitin system. *Nat. Rev. Mol. Cell Biol.* 16, 322–324.
- Ciechanover, A., and Brundin, P. (2003). The ubiquitin proteasome system in neurodegenerative diseases: sometimes the chicken, sometimes the egg. *Neuron* 40, 427–446.
- Cox, J., and Mann, M. (2012). 1D and 2D annotation enrichment: a statistical method integrating quantitative proteomics with complementary high-throughput data. *BMC Bioinformatics* 13 (Suppl 16), S12.

- D'Amico, D., Sorrentino, V., and Auwerx, J. (2017). Cytosolic proteostasis networks of the mitochondrial stress response. *Trends Biochem. Sci.* **42**, 712–725.
- Drews, O., and Taegtmeyer, H. (2014). Targeting the ubiquitin-proteasome system in heart disease: the basis for new therapeutic strategies. *Antioxid. Redox Signal.* **21**, 2322–2343.
- Dulbecco, R., and Freeman, G. (1959). Plaque production by the polyoma virus. *Virology* **8**, 396–397.
- Edgar, D., Shabalina, I., Camara, Y., Wredenberg, A., Calvaruso, M.A., Nijtmans, L., Nedergaard, J., Cannon, B., Larsson, N.G., and Trifunovic, A. (2009). Random point mutations with major effects on protein-coding genes are the driving force behind premature aging in mtDNA mutator mice. *Cell Metab.* **10**, 131–138.
- Emmott, E., Jovanovic, M., and Slavov, N. (2019). Ribosome stoichiometry: from form to function. *Trends Biochem. Sci.* **44**, 95–109.
- Finley, D. (2009). Recognition and processing of ubiquitin-protein conjugates by the proteasome. *Annu. Rev. Biochem.* **78**, 477–513.
- Fredrickson, E.K., and Gardner, R.G. (2012). Selective destruction of abnormal proteins by ubiquitin-mediated protein quality control degradation. *Semin. Cell Dev. Biol.* **23**, 530–537.
- Fu, A., and Danial, N.N. (2018). Grasping for aspartate in tumour metabolism. *Nat. Cell Biol.* **20**, 738–739.
- Grosche, A., Hauser, A., Lepper, M.F., Mayo, R., von Toerne, C., Merl-Pham, J., and Hauck, S.M. (2016). The proteome of native adult Müller glial cells from murine retina. *Mol. Cell. Proteomics* **15**, 462–480.
- Guo, X., Wang, X., Wang, Z., Banerjee, S., Yang, J., Huang, L., and Dixon, J.E. (2016). Site-specific proteasome phosphorylation controls cell proliferation and tumorigenesis. *Nat. Cell Biol.* **18**, 202–212.
- Haack, T.B., Haberberger, B., Frisch, E.-M., Wieland, T., Iuso, A., Gorza, M., Strecker, V., Graf, E., Mayr, J.A., Herberg, U., et al. (2012). Molecular diagnosis in mitochondrial complex I deficiency using exome sequencing. *J. Med. Genet.* **49**, 277–283.
- Haack, T.B., Kopajtich, R., Freisinger, P., Wieland, T., Rorbach, J., Nicholls, T.J., Baruffini, E., Walther, A., Danhauser, K., Zimmermann, F.A., et al. (2013). ELAC2 mutations cause a mitochondrial RNA processing defect associated with hypertrophic cardiomyopathy. *Am. J. Hum. Genet.* **93**, 211–223.
- Hacker, C., and Lucocq, J.M. (2014). Analysis of specificity in immunoelectron microscopy. *Methods Mol. Biol.* **1117**, 315–323.
- Höglinger, G.U., Carrard, G., Michel, P.P., Medja, F., Lombès, A., Ruberg, M., Friguet, B., and Hirsch, E.C. (2003). Dysfunction of mitochondrial complex I and the proteasome: interactions between two biochemical deficits in a cellular model of Parkinson's disease. *J. Neurochem.* **86**, 1297–1307.
- Humphrey, S.J., Karayel, O., James, D.E., and Mann, M. (2018). High-throughput and high-sensitivity phosphoproteomics with the EasyPhos platform. *Nat. Protoc.* **13**, 1897–1916.
- Kaneko, T., Hamazaki, J., Iemura, S., Sasaki, K., Furuyama, K., Natsume, T., Tanaka, K., and Murata, S. (2009). Assembly pathway of the mammalian proteasome base subcomplex is mediated by multiple specific chaperones. *Cell* **137**, 914–925.
- Karamanlidis, G., Lee, C.F., Garcia-Menendez, L., Kolwicz, S.C., Jr., Suthamarak, W., Gong, G., Sedensky, M.M., Morgan, P.G., Wang, W., and Tian, R. (2013). Mitochondrial complex I deficiency increases protein acetylation and accelerates heart failure. *Cell Metab.* **18**, 239–250.
- Karbowsky, M., and Youle, R.J. (2011). Regulating mitochondrial outer membrane proteins by ubiquitination and proteasomal degradation. *Curr. Opin. Cell Biol.* **23**, 476–482.
- Kaupilla, T.E.S., Kaupilla, J.H.K., and Larsson, N.-G.G. (2017). Mammalian mitochondria and aging: an update. *Cell Metab.* **25**, 57–71.
- Kremer, L.S., Bader, D.M., Mertes, C., Kopajtich, R., Pichler, G., Iuso, A., Haack, T.B., Graf, E., Schwarzmayer, T., Terrile, C., et al. (2017). Genetic diagnosis of Mendelian disorders via RNA sequencing. *Nat. Commun.* **8**, 15824.
- Kukat, A., Dogan, S.A., Edgar, D., Mourier, A., Jacoby, C., Maiti, P., Mauer, J., Becker, C., Senft, K., Wibom, R., et al. (2014). Loss of UCP2 attenuates mitochondrial dysfunction without altering ROS production and uncoupling activity. *PLoS Genet.* **10**, e1004385.
- Lavie, J., De Belvalet, H., Sonon, S., Ion, A.M., Dumon, E., Melser, S., Lacombe, D., Dupuy, J.W., Lalou, C., and Bénard, G. (2018). Ubiquitin-dependent degradation of mitochondrial proteins regulates energy metabolism. *Cell Rep.* **23**, 2852–2863.
- Levin, A., Minis, A., Lalazar, G., Rodriguez, J., and Steller, H. (2018). PSMD5 inactivation promotes 26S proteasome assembly during colorectal tumor progression. *Cancer Res.* **78**, 3458–3468.
- Liu, X., Xiao, W., Zhang, Y., Wiley, S.E., Zuo, T., Zheng, Y., Chen, N., Chen, L., Wang, X., Zheng, Y., et al. (2020). Reversible phosphorylation of Rpn1 regulates 26S proteasome assembly and function. *Proc. Natl. Acad. Sci. USA* **117**, 328–336.
- Livnat-Levanon, N., and Glickman, M.H. (2011). Ubiquitin-proteasome system and mitochondria-reciprocity. *Biochim. Biophys. Acta* **1809**, 80–87.
- Livnat-Levanon, N., Kevei, É., Kleifeld, O., Krutauz, D., Segref, A., Rinaldi, T., Erpapazoglou, Z., Cohen, M., Reis, N., Hoppe, T., and Glickman, M.H. (2014). Reversible 26S proteasome disassembly upon mitochondrial stress. *Cell Rep.* **7**, 1371–1380.
- Lokireddy, S., Kukushkin, N.V., and Goldberg, A.L. (2015). cAMP-induced phosphorylation of 26S proteasomes on Rpn6/PSMD11 enhances their activity and the degradation of misfolded proteins. *Proc. Natl. Acad. Sci. USA* **112**, E7176–E7185.
- López-Otín, C., Blasco, M.A., Partridge, L., Serrano, M., and Kroemer, G. (2013). The hallmarks of aging. *Cell* **153**, 1194–1217.
- Meiners, S., Heyken, D., Weller, A., Ludwig, A., Stangl, K., Kloetzel, P.-M.M., and Krüger, E. (2003). Inhibition of proteasome activity induces concerted expression of proteasome genes and de novo formation of mammalian proteasomes. *J. Biol. Chem.* **278**, 21517–21525.
- Meiners, S., Keller, I.E., Semren, N., and Caniard, A. (2014). Regulation of the proteasome: evaluating the lung proteasome as a new therapeutic target. *Antioxid. Redox Signal.* **21**, 2364–2382.
- Münch, C., and Harper, J.W. (2016). Mitochondrial unfolded protein response controls matrix pre-RNA processing and translation. *Nature* **534**, 710–713.
- Pathare, G.R., Nagy, I., Bohn, S., Unverdorben, P., Hubert, A., Körner, R., Nickell, S., Lasker, K., Sali, A., Tamura, T., et al. (2012). The proteasomal subunit Rpn6 is a molecular clamp holding the core and regulatory subcomplexes together. *Proc. Natl. Acad. Sci. USA* **109**, 149–154.
- Rappsilber, J., Mann, M., and Ishihama, Y. (2007). Protocol for micro-purification, enrichment, pre-fractionation and storage of peptides for proteomics using StageTips. *Nat. Protoc.* **2**, 1896–1906.
- Rousseau, A., and Bertolotti, A. (2016). An evolutionarily conserved pathway controls proteasome homeostasis. *Nature* **536**, 184–189.
- Rousseau, A., and Bertolotti, A. (2018). Regulation of proteasome assembly and activity in health and disease. *Nat. Rev. Mol. Cell Biol.* **19**, 697–712.
- Saleem, A., Safdar, A., Kitaoka, Y., Ma, X., Marquez, O.S., Akhtar, M., Nazli, A., Suri, R., Turnbull, J., and Tarnopolsky, M.A. (2015). Polymerase gamma mutator mice rely on increased glycolytic flux for energy production. *Mitochondrion* **21**, 19–26.
- Saxton, R.A., and Sabatini, D.M. (2017). mTOR signaling in growth, metabolism, and disease. *Cell* **168**, 960–976.
- Schapira, A.H., Cooper, J.M., Dexter, D., Jenner, P., Clark, J.B., and Marsden, C.D. (1989). Mitochondrial complex I deficiency in Parkinson's disease. *Lancet* **1**, 1269.
- Schiller, H.B., Fernandez, I.E., Burgstaller, G., Schaab, C., Scheltema, R.A., Schwarzmayer, T., Strom, T.M., Eickelberg, O., and Mann, M. (2015). Time- and compartment-resolved proteome profiling of the extracellular niche in lung injury and repair. *Mol. Syst. Biol.* **11**, 819.
- Schmitt, S., Saathoff, F., Meissner, L., Schropp, E.-M., Lichtmanegger, J., Schulz, S., Eberhagen, C., Borchard, S., Aichler, M., Adamski, J., et al.

- (2013). A semi-automated method for isolating functionally intact mitochondria from cultured cells and tissue biopsies. *Anal. Biochem.* **443**, 66–74.
- Schmitt, S., Eberhagen, C., Weber, S., Aichler, M., and Zischka, H. (2015). Isolation of mitochondria from cultured cells and liver tissue biopsies for molecular and biochemical analyses. *Methods Mol. Biol.* **1295**, 87–97.
- Segref, A., Kevei, É., Pokrzywa, W., Schmeisser, K., Mansfeld, J., Livnat-Levanon, N., Ensenauer, R., Glickman, M.H., Ristow, M., and Hoppe, T. (2014). Pathogenesis of human mitochondrial diseases is modulated by reduced activity of the ubiquitin/proteasome system. *Cell Metab.* **19**, 642–652.
- Semren, N., Welk, V., Korfei, M., Keller, I.E., Fernandez, I.E., Adler, H., Günther, A., Eickelberg, O., and Meiners, S. (2015). Regulation of 26S proteasome activity in pulmonary fibrosis. *Am. J. Respir. Crit. Care Med.* **192**, 1089–1101.
- Sha, Z., and Goldberg, A.L. (2014). Proteasome-mediated processing of Nrf1 is essential for coordinate induction of all proteasome subunits and p97. *Curr. Biol.* **24**, 1573–1583.
- Shim, S.M., Lee, W.J., Kim, Y., Chang, J.W., Song, S., and Jung, Y.K. (2012). Role of S5b/PSMD5 in proteasome inhibition caused by TNF- α /NF κ B in higher eukaryotes. *Cell Rep.* **2**, 603–615.
- Smith, A.C., and Robinson, A.J. (2016). MitoMiner v3.1, an update on the mitochondrial proteomics database. *Nucleic Acids Res.* **44** (D1), D1258–D1261.
- Spinelli, J.B., and Haigis, M.C. (2018). The multifaceted contributions of mitochondria to cellular metabolism. *Nat. Cell Biol.* **20**, 745–754.
- Steffen, J., Seeger, M., Koch, A., and Krüger, E. (2010). Proteasomal degradation is transcriptionally controlled by TCF11 via an ERAD-dependent feedback loop. *Mol. Cell* **40**, 147–158.
- Suhm, T., Kaimal, J.M., Dawitz, H., Peselj, C., Masser, A.E., Hanzén, S., Ambrožič, M., Smiałowska, A., Björck, M.L., Brzezinski, P., et al. (2018). Mitochondrial translation efficiency controls cytoplasmic protein homeostasis. *Cell Metab.* **27**, 1309–1322.e6.
- Sullivan, L.B., Gui, D.Y., Hosios, A.M., Bush, L.N., Freinkman, E., and Vander Heiden, M.G. (2015). Supporting aspartate biosynthesis is an essential function of respiration in proliferating cells. *Cell* **162**, 552–563.
- Sullivan, L.B., Gui, D.Y., and Vander Heiden, M.G. (2016). Altered metabolite levels in cancer: implications for tumour biology and cancer therapy. *Nat. Rev. Cancer* **16**, 680–693.
- Trifunovic, A., Hansson, A., Wredenberg, A., Rovio, A.T., Dufour, E., Khvorostov, I., Spelbrink, J.N., Wibom, R., Jacobs, H.T., and Larsson, N.-G. (2005). Somatic mtDNA mutations cause aging phenotypes without affecting reactive oxygen species production. *Proc. Natl. Acad. Sci. USA* **102**, 17993–17998.
- Tsvetkov, P., Mendillo, M.L., Zhao, J., Carette, J.E., Merrill, P.H., Cikes, D., Varadarajan, M., van Diemen, F.R., Penninger, J.M., Goldberg, A.L., et al. (2015). Compromising the 19S proteasome complex protects cells from reduced flux through the proteasome. *eLife* **4**, 1–22.
- Tsvetkov, P., Sokol, E., Jin, D., Brune, Z., Thiru, P., Ghandi, M., Garraway, L.A., Gupta, P.B., Santagata, S., Whitesell, L., and Lindquist, S. (2017). Suppression of 19S proteasome subunits marks emergence of an altered cell state in diverse cancers. *Proc. Natl. Acad. Sci. USA* **114**, 382–387.
- Tsvetkov, P., Detappe, A., Cai, K., Keys, H.R., Brune, Z., Ying, W., Thiru, P., Reidy, M., Kugener, G., Rossen, J., et al. (2019). Mitochondrial metabolism promotes adaptation to proteotoxic stress. *Nat. Chem. Biol.* **15**, 681–689.
- Tyanova, S., Temu, T., and Cox, J. (2016). The MaxQuant computational platform for mass spectrometry-based shotgun proteomics. *Nat. Protoc.* **11**, 2301–2319.
- Vabulas, R.M., and Hartl, F.U. (2005). Protein synthesis upon acute nutrient restriction relies on proteasome function. *Science* **310**, 1960–1963.
- VerPlank, J.J.S., and Goldberg, A.L. (2017). Regulating protein breakdown through proteasome phosphorylation. *Biochem. J.* **474**, 3355–3371.
- VerPlank, J.J.S., Lokireddy, S., Zhao, J., and Goldberg, A.L. (2019). 26S Proteasomes are rapidly activated by diverse hormones and physiological states that raise cAMP and cause Rpn6 phosphorylation. *Proc. Natl. Acad. Sci. USA* **116**, 4228–4237.
- Vilchez, D., Boyer, L., Morante, I., Lutz, M., Merkwirth, C., Joyce, D., Spencer, B., Page, L., Masliah, E., Berggren, W.T., et al. (2012). Increased proteasome activity in human embryonic stem cells is regulated by PSMD11. *Nature* **489**, 304–308.
- Walerych, D., Lisek, K., Sommaggio, R., Piazza, S., Ciani, Y., Dalla, E., Rajkowska, K., Gaweda-Walerych, K., Ingallina, E., Tonelli, C., et al. (2016). Proteasome machinery is instrumental in a common gain-of-function program of the p53 missense mutants in cancer. *Nat. Cell Biol.* **18**, 897–909.
- Wang, X., and Chen, X.J. (2015). A cytosolic network suppressing mitochondria-mediated proteostatic stress and cell death. *Nature* **524**, 481–484.
- Wang, X., Meul, T., and Meiners, S. (2020). Exploring the proteasome system: a novel concept of proteasome inhibition and regulation. *Pharmacol. Ther.* **211**, 107526.
- Wiśniewski, J.R., Zougman, A., Nagaraj, N., and Mann, M. (2009). Universal sample preparation method for proteome analysis. *Nat. Methods* **6**, 359–362.
- Wrobel, L., Topf, U., Bragoszewski, P., Wiese, S., Sztolsztener, M.E., Oeljeklaus, S., Varabyova, A., Lirski, M., Chroscicki, P., Mroczek, S., et al. (2015). Mistargeted mitochondrial proteins activate a proteostatic response in the cytosol. *Nature* **524**, 485–488.
- Zhang, Y., Nicholatos, J., Dreier, J.R., Ricoult, S.J.H., Widenmaier, S.B., Hottamisligil, G.S., Kwiatkowski, D.J., and Manning, B.D. (2014). Coordinated regulation of protein synthesis and degradation by mTORC1. *Nature* **513**, 440–443.
- Zischka, H., Larochette, N., Hoffmann, F., Hamöller, D., Jägemann, N., Lichtmannegger, J., Jennen, L., Müller-Höcker, J., Roggel, F., Göttlicher, M., et al. (2008). Electrophoretic analysis of the mitochondrial outer membrane rupture induced by permeability transition. *Anal. Chem.* **80**, 5051–5058.
- Zukunft, S., Sorgenfrei, M., Prehn, C., Möller, G., and Adamski, J. (2013). Targeted metabolomics of dried blood spot extracts. *Chromatographia* **76**, 1295–1305.

STAR★METHODS

KEY RESOURCES TABLE

REAGENT or RESOURCE	SOURCE	IDENTIFIER
Antibodies		
Mouse monoclonal anti- α 1-7	Abcam	Cat#ab22674; RRID:AB_2171376
Rabbit polyclonal anti-Rpn6	Novus	Cat#NBP1-46191; RRID:AB_10009423
Rabbit polyclonal anti-Rpn4	Abcam	Cat#ab103408; RRID:AB_10861889
Rabbit monoclonal anti-p28	Abcam	Cat#ab182576; RRID:AB_2687444
Rabbit polyclonal anti-phospho p70 S6 kinase	Cell Signaling	Cat#9208; RRID:AB_330990
Rabbit monoclonal Anti-phospho S6 ribosomal protein	Cell Signaling	Cat#4858; RRID:AB_916156)
Chemicals, Peptides, and Recombinant Proteins		
Aspartate	Sigma Aldrich	A7219; CAS: 56-84-8
Pyruvate	AppliChem	A4859; CAS: 113-24-6
Rapamycin	Sigma Aldrich	553210; CAS: 53123-88-9
Metformin hydrochloride	Sigma Aldrich	PHR1084; CAS:1115-70-4
Thiazolyl Blue Tetrazolium Bromide (MTT)	Sigma Aldrich	M5655; CAS: 298-93-1
Substrate for Native gel activity assay: Suc-Leu-Leu-Val-Tyr-AMC	Bachem	I-1395.0100; CAS: 94367-21-2
Velcade® (Bortezomib) 3.5 mg Single Use Vial for Injection	MILLENIUM Pharmaceuticals	N/A
Critical Commercial Assays		
NAD/NADH Glo™ assay	Promega	G9071
CellTiter Glo™ ATP assay	Promega	G9241
Proteasome Glo™ assay (Chymotrypsin-like)	Promega	G8621
Proteasome Glo™ assay (Trypsin-like)	Promega	G8631
Proteasome Glo™ assay (Caspase-like)	Promega	G8641
Click-iT Plus OPP Protein Synthesis Assay Kit	Life Technologies	C10456
Deposited Data		
Proteomics Data from WT/mutator MEFs	This paper	Pride: PXD019695
Proteomics Data from WT/mutator mitochondria	This paper	Pride: PXD019695
Phosphoproteomics Data from mutator MEFs	This paper	Pride: PXD019697
Metabolomics Data from WT/mutator MEFs	This paper	BioStudies: S-BSST444
RNA sequencing data from WT/mutator MEFs	This paper	GEO: GSE153983
Experimental Models: Cell Lines		
WT/mutator mouse embryonic fibroblasts (MEFs) IDs: WT: 56, 59, 69; Mutator: 49, 50, 53, 68	Laboratory of Aleksandra Trifunovic	N/A
Primary human ND5 skin fibroblasts	Laboratory of Holger Prokisch	ID: 67333
Primary human lung fibroblasts	Laboratory of Andreas Günther	ID: 409Sp
Oligonucleotides		
Primer for RT-qPCR, see table Primer sequences for qRT-PCR	This paper	N/A
siRNAs for silencing experiments, see siRNA Mediated Gene Silencing	This paper	N/A

(Continued on next page)

Continued

REAGENT or RESOURCE	SOURCE	IDENTIFIER
Software and Algorithms		
GraphPad Prism 5 and 7	GraphPad Software	N/A
Image Lab	Bio-Rad	N/A

RESOURCE AVAILABILITY

Lead Contact

Further information and requests for resources and reagents should be directed to and will be fulfilled by the lead contact Silke Meiners (silke.meiners@helmholtz-muenchen.de).

Materials Availability

This study did not generate new unique reagents.

Data and Code Availability

Data deposition: The mass spectrometry data of this study have been deposited in the ProteomeXchange Consortium at <https://proteomecentral.proteomexchange.org/cgi/GetDataset> using the dataset identifier PXD019695 (proteomics data), PXD019697 (phospho-proteomics data). Metabolomics data have been deposited at BioStudies (Identifier: S-BSST444). RNA sequencing data have been deposited at GEO <https://www.ncbi.nlm.nih.gov/geo/> (Identifier: GSE153983).

EXPERIMENTAL MODEL AND SUBJECT DETAILS

Cell culture

Mouse embryonic fibroblasts from mtDNA mutator mice were generated as previously described (Kukat et al., 2014). Wild-type (WT) and mutator MEFs were cultured in DMEM High Glucose (4.5 g/l) medium (without Sodium pyruvate and L-glutamine) (ThermoFisher Scientific, Rockford, USA) supplemented with 10% (v/v) fetal bovine serum (FBS) (Biochrome), 100 U/mL penicillin/streptomycin (GIBCO, Thermo Fisher Scientific) and 4 mM L-glutamine (Thermo Fisher Scientific) at 37°C and 5% CO₂. MEFs isolated from four individual mtDNA mutator and three individual WT mice were used as different biological replicates (Trifunovic et al., 2005). The different cell lines have the following identifiers and genders: WT: 56 (female), 59 (male), 69 (male); Mutator: 49 (female), 50 (female), 53 (female), 68 (male). Primary skin fibroblasts were obtained from Holger Prokisch (Institute of Neurogenomics, Helmholtz Zentrum München, Munich, Germany). Skin fibroblasts derived from a healthy donor and from a patient with a mutation in the ND5 gene, which encodes for a mitochondrial complex I subunit. Further information about the donors are not available. Skin fibroblasts were cultured in DMEM High Glucose (4.5 g/l) medium (without sodium pyruvate and L-glutamine) (ThermoFisher Scientific, Rockford, USA) supplemented with 10% FBS, 100 U/mL penicillin/streptomycin, 4 mM L-glutamine (Thermo Fisher Scientific) and 200 μM uridine (Sigma) at 37°C and 5% CO₂. Cells were grown to approx. 70% confluency before passaging them into new flasks or using them for experiments. Primary human lung fibroblasts (ID: 409Sp; Male, 51 years, peripheral normal lung tissue, organ donor) were cultured in DEMEM High Glucose (4.5 g/l) medium (without sodium pyruvate and L-glutamine) (ThermoFisher Scientific, Rockford, USA) supplemented with 10% FBS, 100 U/mL penicillin/streptomycin, 4 mM glutamine (ThermoFisher), 2 ng/ml β-FGF (ThermoFisher), 0.5 ng/ml EGF (Sigma-Aldrich) and 5 μg/ml insulin (ThermoFisher).

METHOD DETAILS

Protein extraction

To preserve proteasome activity native protein lysates were prepared. Cell pellets were resuspended in TSDG buffer (10 mM Tris/HCl, 25 mM KCl, 1.1 mM MgCl₂, 0.1 mM EDTA, 1 mM DTT, 1 mM NaN₃, 10% glycerol, pH 7) containing complete protease inhibitor (Roche Diagnostics, Basel, Switzerland) and phosphatase inhibitor (PhosStop, Roche Diagnostics). Cell suspensions were subjected to seven cycles of freezing in liquid nitrogen and thawing at room temperature. Cell debris was removed by centrifugation and protein concentration in the supernatant was assessed using the Pierce BCA protein assay (ThermoFisher Scientific).

Proteasome activity assays

In order to determine the activity of the three 20S proteasome active sites namely chymotrypsin-like (CT-L), caspase-like (C-L) and trypsin-like (T-L) the Proteasome-Glo Assay (Promega, Fitchburg, USA) was applied according to the manufacturer's instructions.

Here, 1 μ g protein (TSDG lysates) per sample was first diluted with TSDG buffer to obtain equal volumes of TSDG buffer in each sample and then adjusted to a final volume of 20 μ L with water. The prepared dilutions were transferred to white flat bottom 96-well plates and mixed with 20 μ L of the respective active site specific substrate Suc-LLVY-aminoluciferin (CT-L specific), Z-nLPnLD-aminoluciferin (C-L specific) and Z-LRR-aminoluciferin (T-L specific). The different peptide substrates are cleaved by the respective proteasome active site and the released aminoluciferin serves as a substrate for the luciferase contained in the reaction buffer to generate a luminescent signal. This light signal was measured every 5 min for 1 h during the reaction in a Tristar LB 941 plate reader (Berthold Technologies, Bad Wildbad, Germany). For each substrate the samples were measured in technical triplicates.

Western blot analysis

For western blot analysis, 15 μ g of protein lysates were mixed with 6x Laemmli buffer (300 mM Tris, 50% Glycerol, 6% SDS, 0.01% Bromphenol blue, 600 mM DTT) and incubated at 95°C for 5 min. After the incubation, samples were subjected to electrophoresis on 10 - 15% SDS-PAGE gels and blotted onto polyvinylidene difluoride (PVDF) membranes. Electrophoretic separation was performed at 90 - 130 V at room temperature and transfer to PVDF membranes was performed at 250 mA for 90 min at 4°C. Membranes were blocked using Rotiblock (Roth, Karlsruhe, Germany) and treated with primary antibodies overnight at 4°C and subsequently with secondary antibodies (1:40.000) for 1 h at room temperature. Antibodies used were: Anti- α 1-7 (1:1000, Abcam Cat# ab22674, RRID:AB_2171376), Anti-Rpn6 (1:1000, Novus Cat# NBP1-46191, RRID:AB_10009423), Anti- β 5 (1:1000, Abcam Cat# ab90867, RRID:AB_10675505), Anti-Rpt5 (1:1000, Bethyl Cat# A303-538A, RRID:AB_10953858), Rpn8 (1:1000, Abcam Cat# ab11436, RRID:AB_298041), Anti-S5b (1:1.000, Abcam Cat# ab137733), Anti-Rpn4 (1:1.000, Abcam Cat# ab103408, RRID:AB_10861889), Anti-p28 (1:1.000, Abcam Cat# ab182576, RRID:AB_2687444), Anti-S6 kinase (1:2.000, Cell Signaling Technology Cat# 2708, RRID:AB_39072), Anti-phospho p70 S6 kinase (1:2.000, Cell Signaling Technology Cat# 9208, RRID:AB_330990), Anti-S6 ribosomal protein (1:2.000, Cell Signaling Technology Cat# 2317, RRID:AB_2238583), Anti-phospho S6 ribosomal protein (1:2.000, Cell Signaling Technology Cat# 4858, RRID:AB_916156), Anti-Raptor (Cell Signaling Technology Cat# 2280, RRID:AB_561245), Anti-K48-Ubiquitin (1:3000, Millipore Cat# 05-1307, RRID:AB_1587578), HRP-conjugated anti- β -Actin (1:40.000, Sigma-Aldrich Cat# A3854, RRID:AB_262011), HRP-conjugated anti-GAPDH (1:20.000, Cell Signaling Technology Cat# 5014, RRID:AB_10693448), Anti-OxPhos Rodent WB Antibody Cocktail (1:1.000, Thermo Fisher Scientific Cat# 45-8099, RRID:AB_2533835), Anti-mouse IgG HRP-linked (1:40.000, Cell Signaling Technology Cat# 7076, RRID:AB_330924), Anti-rabbit IgG HRP-linked (1:40.000, Cell Signaling Technology Cat# 7074, RRID:AB_2099233).

Native gel analysis

15 μ g protein of TSDG lysates were diluted with TSDG buffer to the highest sample volume. The diluted lysates were mixed with 5x native loading buffer (250 mM Tris, 50% Glycerol, 0.01% Bromphenol blue) and were loaded onto commercially available 3%-8% gradient NuPAGE Novex Tris-acetate gels (Life Technologies, Darmstadt, Germany). Native proteasome complexes were separated at 150 V for 4 h at 4°C. After native gel electrophoresis the CT-L activity of the separated native proteasome complexes was determined by an in-gel substrate overlay proteasome activity assay. For this purpose gels were incubated for 30 min at 37°C in a buffer containing 50 mM Tris, 1 mM ATP, 10 mM MgCl₂, 1 mM DTT and 0.05 mM Suc-LLVY-AMC (Bachem, Bubendorf, Switzerland). Fluorescence generated by the CT-L specific cleavage of the fluorogenic Suc-LLVY-AMC peptide substrate in the active proteasome was detected within the gel at an excitation wavelength of 380 nm and emission wavelength of 460 nm using the ChemiDoc XRS+ system (BioRad, Hercules, USA). Finally, the gels were incubated for 15 min in a solubilization buffer (66 mM Na₂CO₃, 2% SDS, 1.5% β -mercaptoethanol) at room temperature in order to facilitate the subsequent blotting of the proteins using the previously described western blot technique.

Primer sequences for qRT-PCR

Gene	Forward Primer (5'-3')	Reverse Primer (5'-3')
PsmA3	agatggtgtgtcttgggg	aacgagcatctgccaaca
PsmB5	TCAGTGATGGTCTGAGCCTG	CCATGGTGCCTAGCAGGTAT
PsmB6	CAGAACAACCACTGGGTCCT	CCCGGTATCGGTAACACATC
PsmB7	TCGCTGGGGTGGTCTATAAG	TCCCAGCACCAACAATAA
PsmC3	GTGAAGGCCATGGAGGTAGA	GTTGGATCCCCAAGTTCTCA
PsmD11	GCTCAACACCCAGAAGATGT	AGCCTGAGCCACGCATTTTA
PsmD5	TGTGAGCGCTACCCTGTTTT	TTCAGCTCCGTGGAAGCATT
PsmD9	TAGAAGCGCAGATCAAGGCC	TGTCACATTGAGGGGCTTCC
PsmD10	TTGAAGGAGCGCATTTTGGC	GAGACCAACCTGCGTCATCT
L19 Rpl19 (housekeeper)	TGTACCTGAAGGTGAAGGGG	GCGTGCTTCCTTGGTCTTAG

Quantitative real-time RT-PCR

Total RNA isolation was performed by phenol/chloroform extraction using the Roti-Quick-Kit (Roth, Karlsruhe, Germany). 1 μ g RNA per sample was transcribed into cDNA by M-MLV reverse transcriptase (Sigma Aldrich, Taufkirchen, Germany). The obtained cDNA was applied for quantitative RT-PCR with the SYBR Green LC480 System (Roche Diagnostic, Mannheim, Germany) using the respective forward and reverse primers for the genes of interest (Psm3, Psm5, Psm6, Psm7, Psmc3, Psm11, Psm5, Psm9, Psm10) at a concentration of 2 pM. All samples were measured in technical duplicates.

Measurement of ATP levels

Cellular ATP levels were determined using the CellTiter-Glo assay kit (Promega, Madison, WI, USA). Cells were seeded in 6-well plates and cultured for 24 h. After the treatment cells were harvested with trypsin and 40,000 cells/well were transferred to a white flat bottom 96-well plate. CellTiter-Glo reagent was added and the luminescent signal was measured after 3 min at a time for 30 min in total in a Tristar LB 941 plate reader (Berthold Technologies).

Analysis of reactive oxygen species (ROS) in cells

Mitochondrial superoxide generation was analyzed using the MitoSOX[®] Red probe (Life Technologies) and overall cellular ROS generation was analyzed by H₂DCFDA (ThermoFisher Scientific) fluorescence. For fluorescence analysis cells were seeded in 6-well plates and grown for 24 h. Cells were then stained for 30 minutes in medium containing 5 μ M MitoSOX[®] Red or 25 μ M H₂DCFDA, respectively. Cells were washed with PBS, trypsinized, and resuspended in 500 μ l FACS Buffer (PBS, 2% FBS, 20 μ M EDTA). Samples were then analyzed by flow cytometry using a BD LSRII Flow Cytometer (BD Biosciences, Heidelberg, Germany) and mean fluorescence intensity was measured.

Cellular oxygen consumption

Oxygen consumption in mtDNA mutator MEFs was measured using a Seahorse XF analyzer (Seahorse Bioscience) and oxygen consumption values were normalized to cell number as assessed by the CyQuant assay kit (Life technologies) (Haack et al., 2012). Oxygen consumption was measured at basal conditions (basal respiration) after addition of 1 μ M oligomycin (blocking proton backflow through complex V to measure proton leak), upon addition of 1 μ M CCCP (uncoupling the respiratory chain to enable unlimited proton flow through the mitochondrial membrane to induce maximum respiration) and after addition of 2 μ M rotenone/antimycin A (blocking complex I and III to inhibit mitochondrial respiration). Non-mitochondrial respiration was subtracted from all values.

Mitochondrial cytochrome c staining

To analyze the mitochondrial network in WT and mutator MEFs, cells were seeded on 15 mm glass coverslips and cultured to 50% confluency. Cells were then fixed on the coverslips using 4% paraformaldehyde for 10 min. Permeabilization was performed with 0.1% Triton-X in PBS for 15 min and unspecific binding sites were blocked with Roti-Immunoblock (Roth, Karlsruhe, Germany) for 1 h at room temperature. Cells were then incubated with anti-cytochrome c antibody (1:1,000, BD Bioscience, San Jose, CA, USA) for 2 h at room temperature. The secondary Alexa Fluor[®] (AF)-488-coupled antibody (1:750, Life Technologies) was added for 1 h at room temperature. After 2 washing steps in PBS cells were stained with 4',6-Diamidin-2-phenylindol (DAPI) (Sigma-Aldrich) for 5 min. For confocal laser microscopy (Zeiss LSM710, Oberkochen, Germany) cells were mounted on microscopic slides using DAKO mounting medium.

Isolation of mitochondria

Mitochondria from cultured cells were isolated as previously described (Schmitt et al., 2013). Briefly, cells were resuspended in isolation buffer (300 mM sucrose, 5 mM TES, 200 μ M EGTA, pH 7.2, without BSA) to a concentration of $5-7 \times 10^6$ cells per ml and pumped 4 times through a clearance of 6 μ m (flow rate 700 μ l/min). The homogenate was centrifuged at 800 x g (4°C) to remove nuclei and cell debris and mitochondria were pelleted at 10,000 x g. For purification, mitochondria were loaded on a Nycodenz[®] (Axis Shield PoC AS, Oslo, Norway) density gradient (24%/18%) and centrifuged at 30,000 rpm for 15 min at 4°C in a Beckman ultracentrifuge (rotor SW 55.Ti). Mitochondria were collected at the 24%/18% interphase and washed once in isolation buffer without BSA (9,000 x g, 10 min at 4°C).

Electron microscopy

Electron microscopy of cells and there from isolated mitochondria was done as previously described (Zischka et al., 2008). Samples were fixed with 2.5% glutaraldehyde in 0.1 M sodium cacodylate buffer, pH 7.4 (Electron Microscopy Sciences, Hatfield, USA) for 24 h at minimum. Thereafter glutaraldehyde was removed and samples were washed three times with 0.1 M sodium cacodylate buffer, pH 7.4. Postfixation and prestaining was done for 45 to 60 min with 1% osmium tetroxide (10 mL 4% osmium tetroxide (Electron Microscopy Sciences, cat no. 19190, Hatfield, USA), 10 mL ddH₂O, 10 mL 3.4% sodium chloride and 10 mL 4.46% potassium dichromate (pH adjusted to 7.2 with KOH (Sigma Aldrich)). Samples were washed three times with ddH₂O and dehydrated with an ascending ethanol series (15 min with 30%, 50%, 70%, 90% and 96%, respectively and two times 10 min with 100%) and propylene oxide (two times 30 min, Serva Electrophoresis GmbH, Heidelberg, Germany). Subsequently, samples were embedded in Epon (3.61 M glycidether 100, (Serva Electrophoresis GmbH), 1.83 M methylnadicanhydride (Serva Electrophoresis GmbH),

0.92M dodecenylsuccinic anhydride (Serva Electrophoresis GmbH), 5.53 mM 2,4,6-Tris(dimethylaminomethyl)phenol (Serva Electrophoresis GmbH). Ultrathin sections were automatically stained with UranylLess EM Stain (Electron Microscopy Sciences) and 3% lead citrate (Leica, Wetzlar, Germany) using the contrasting system Leica EM AC20 (Leica, Wetzlar, Germany) and examined with a JEOL –1200 EXII transmission electron microscope at 80 kV (JEOL GmbH, Freising, Germany). Images were taken using a digital camera (KeenViewII, Olympus, Germany) and processed with the iTEM software package (anlySISFive; Olympus, Germany).

Measurement of cellular NADH levels

Cellular NADH levels in WT and mutator MEFs were determined using the NAD/NADH-Glo assay kit (Promega) according to the manufacturer's instructions. Cells were trypsinized and washed with PBS. 40000 cells per sample (triplicates) dissolved in 50 μ L PBS were transferred in a 96-well plate. Cell lysis was performed using 50 μ L 0.2 M NaOH with 1% Dodecyltrimethylammonium bromide (DTAB). Cells were incubated at 60°C for 15 min to deplete NAD⁺ from the lysates. 50 μ L 0.25 M Tris, 0.2 M HCl solution was added to the wells. 20 μ L of each well were transferred into a white flat bottom 96-well plate and mixed with 20 μ L NAD/NADH Glo detection reagent. Obtained luminescence was measured in a Tristar LB 941 plate reader.

Metabolomic analysis

Wild-type and mutator MEFs were seeded in 6 well plates for a final cell number of around 1×10^6 cells after 24 h. 6 wells per cell line were used for metabolomics analysis and 6 additional wells were counted to determine the final cell number of each cell line. Cells were first washed two times with PBS and then overlaid with 300 μ L dry ice cold methanol. Cells of each well were harvested by scraping and transferred into a 0.5 mL PP-Sarstedt Micro tube (Sarstedt AG & Co, Nümbrecht, Germany) and frozen immediately on dry ice. Samples were stored at –80°C until metabolomics analysis. Targeted metabolomics analysis was performed at the Helmholtz Zentrum München, Institute of Experimental Genetics, Genome Analysis Center in Neuherberg, Germany. Metabolites were quantified using the Absolute/DQ™ Kit p180 (BIOCRATES Life Sciences AG, Innsbruck, Austria) and LC-ESI-MS/MS and FIA-ESI-MS/MS measurements as described previously (Zukunft et al., 2013). The method of Absolute/DQ™ p180 Kit has been proven to be in conformance with the EMEA-Guideline "Guideline on bioanalytical method validation (https://www.ema.europa.eu/ema/index.jsp?curl=pages/includes/document/document_detail.jsp?webContentId=WC500109686%26mid=WC0b01ac058009a3dc), which implies proof of reproducibility within a given error range. To each sample, 80 mg glass beads were added. Samples were homogenized using a Precellys24 (PeqLab Biotechnology, Erlangen, Germany) at 4°C for two times over 25 s at 5500 rpm and centrifuged at 4°C and $10,000 \times g$ for 5 min. 10 μ L of the supernatants were directly applied to the assay.

Sample handling was performed by a Hamilton Microlab STAR™ robot (Hamilton Bonaduz AG, Bonaduz, Switzerland) and a Ultra-vap nitrogen evaporator (Porvair Sciences, Leatherhead, UK), beside standard laboratory equipment. Mass spectrometric analyses were done on an API 4.000 triple quadrupole system (Sciex Deutschland GmbH, Darmstadt, Germany) equipped with a 1200 Series HPLC (Agilent Technologies Deutschland GmbH, Böblingen, Germany) and a HTC PAL auto sampler (CTC Analytics, Zwingen, Switzerland) controlled by the software Analyst 1.6.2. Data evaluation for quantification of metabolite concentrations and quality assessment was performed with the software MultiQuant 3.0.1 (Sciex) and the Met/DQ software package, which is an integral part of the Absolute/DQ Kit. Metabolite concentrations were calculated using internal standards and reported in μ M.

Aspartate and pyruvate supplementation

Aspartate medium was freshly prepared for each experiment. For this purpose 10 mM aspartate (Sigma Aldrich, Taufkirchen, Germany) was dissolved in DMEM High Glucose medium. To avoid effects on the cells through an acidification of the medium by aspartate, the pH of the medium was adjusted to 7.5 using 5 M NaOH. The medium was then sterile filtered with sterile, non-pyrogenic, hydrophilic filters (VWR) and 10% FCS was added. 1 mM pyruvate (Sigma Aldrich, Taufkirchen, Germany) was dissolved in medium. Pyruvate-supplemented medium was then sterile filtered and added to the cells.

Metformin treatment

An optimal non-toxic metformin (Sigma Aldrich) concentration was titrated for each cell line (WT MEFs: 5 mM, skin fibroblasts: 4 mM, lung fibroblasts: 4 mM). Metformin was then directly added to the respective aspartate- or pyruvate-containing medium. Cells were incubated with metformin for 72 h. Cell number and proteasome activity after 72 h were used as a read out.

Lysate preparation for phosphoproteome analysis (Humphrey et al., 2018)

Mutator cells (300.000 cells per well) were seeded in a 6 well plate the day before treatment. Cells were treated with 10 mM aspartate for 4 h. Pre-chilled (4°C) Sodium deoxycholate (SDC) lysis buffer (4% (w/v) SDC, 100 mM Tris -HCl pH 8.5) was added to the cells and scraped off. To inactivate endogenous proteases and phosphatases and ease lysis the lysates were heated to 95°C for 5 min. The lysates were homogenized at 4°C with the Bioruptor (Diagenode) (2 cycles at maximum output power). To determine the protein concentration BCA assays were performed and the lysates were diluted to identical protein concentrations of appropriate starting material in a final volume of 270 μ L SDC lysis buffer. Reduction of caramidomethylate cysteine residues and disulphide bonds was performed by adding 30 μ L of reduction/alkylation buffer in a ratio 1:10 to the lysates and incubation for 5 min, at 45°C and 1500 rpm. After lysates had been cooled down to RT, the enzymes lys-C (Wako) and trypsin (Sigma) were added (ratio of 1:100) and digestion was carried out overnight at 37°C with shaking (1500 rpm).

Phosphopeptide enrichment

C8 StageTips (Supelco) (were prepared for each sample as described in the protocol by [Rappsilber et al. \(2007\)](#). Before adding 100 μ L EP enrichment buffer (48% (vol/vol) Trifluoroacetic acid (TFA), 8 mM KH_2PO_4) to the samples (mix 1.500 rpm, 30 s), 400 μ L isopropanol was added and mixed for 30 s, 1.500 rpm to prevent precipitation. The ratio of TiO_2 beads to protein should be 12:1 (wt:wt). The beads were resuspended in EP loading buffer (6% (vol/vol) TFA/80% (vol/vol) acetonitrile (ACN)) at a concentration of 1 mg/ μ L and an aliquot of suspended beads was pipetted to the samples and the samples were shaken for 5 min, 40°C, 2.000 rpm. The beads were pelleted via centrifugation at 2.000 g for 1 min. The supernatant (the non-phosphopeptides) was discarded. The pellets were washed 4x with 1 mL EP wash buffer (5% (vol/vol) TFA/60% isopropanol (vol/vol)) by shaking at RT for 30 s, 2000 rpm. After each washing step the beads were pelleted (2.000 g, 1 min) and the supernatant was discarded. After the final washing step the beads were resuspended in 75 μ L EP transfer buffer (0.1% TFA/60% (vol/vol) isopropanol) and transferred onto the top of a C8 StageTip. To ensure all beads were transferred from the vial another 75 mL EP transfer buffer were added to each sample and transferred to the C8 StageTip. The StageTips were then centrifuged at 1500 g for 8 min at RT to dryness to pack the TiO_2 beads on the top of the C8 material. Elution of the phosphopeptides was conducted with 30 μ L EP elution buffer (200 μ L of ammonia solution (NH_4OH) added to 800 μ L of 40% (vol/vol) ACN/acetonitrile) and centrifugation at 1500 g, 4 min at RT to dryness. The eluates were collected into clean PCR strip tubes and elution was repeated with 30 μ L EP elution buffer into the same tubes. The tubes were then placed into an evaporative concentrator and concentrated under vacuum at 45°C until ~15 μ L sample remained.

StageTip desalting of phosphopeptides

SDB-RPS StageTips (Supelco) were prepared for each sample as described in the protocol by [Rappsilber et al. \(2007\)](#). 100 μ L of SDB-RPS loading buffer (1% (vol/vol) TFA in isopropanol) were added to each sample and then transferred onto the top of a SDB-RPS StageTip. Centrifugation was carried out at 1500 g for 8 min, RT until dryness using the adaptor for the StageTips. StageTips were washed with SDB-RPS wash buffer 1 (1% (vol/vol) TFA in isopropanol) and centrifuged until dryness at 1500 g, 8 min, RT. Next, one washing step with SDB-RPS wash buffer 2 (0.2% (vol/vol) TFA/5% (vol/vol) ACN) was performed. By addition of 60 μ L SDB-RPS elution buffer (Add 20 μ L of ammonia solution (NH_4OH) to 4 mL of 60% (vol/vol) ACN) the phosphopeptides were eluted (1500 g, 5 min, RT) and collected into clean PCR strip tubes. Under vacuum at 45°C the samples were dried in an evaporative concentrator. Samples were resuspended in 7 μ L MS loading buffer (0.1% TFA/2% (vol/vol) ACN) by incubation in a sonicating water bath on low power for 5 min. Afterward phosphopeptides were spun down at 2000 g for 1 min at RT. Detection of phosphopeptides via Mass spectrometry was performed according to the EasyPhos protocol.

Bioinformatic analysis of phosphoproteomics data

The Phospho(STY)Sites.txt file of the MaxQuant output was used for analysis with Perseus (version 1.6.5.0). The table was filtered to retain only these sites that have a localization probability > 0.75. The data was log2 transformed and entries from reverse data base hits and potential contaminants were filtered out. Protein annotations were added and the data was filtered to have at least three out of four quantified values in either the WT or the mutator group. The data was normalized. Zero values were imputed with a normal distribution of artificial values generated at 1.6 standard deviations, subtracted from the mean, of the total intensity distribution and a width of 0.3 standard deviations. To identify significantly regulated phosphosites a Student's t test was performed ($S_0 = 1$, FDR 0.1). Fisher exact test (FDR > 0.02) was used to find enriched kinase motifs in the regulated phosphosites. The fisher exact test determines if there are non-random associations between a categorical column and all terms in the other categorical columns.

Filter-aided sample preparation for proteomic analysis

Protein content was determined using the Pierce BCA protein assay (Thermo Scientific, Rockford, USA) and 10 μ g RIPA protein lysate (50 mM Tris, 150 mM NaCl, 1% NP-40, 0.5% Sodium deoxycholate, 0.1% SDS) was subjected to tryptic digest using a modified filter-aided sample preparation (FASP) protocol ([Grosche et al., 2016](#); [Wiśniewski et al., 2009](#)). Peptides were collected by centrifugation and acidified with 2 μ L 100% trifluoroacetic acid prior to mass spectrometric analysis.

Proteomic analysis

For LC-MS/MS acquisition a QExactive HF mass spectrometer (ThermoFisher Scientific, Dreieich, Germany) coupled to a RSLC system (ThermoFisher Scientific) was used. Approx. 0.5 μ g of peptides were automatically loaded to the HPLC system equipped with a nano trap column (300 μ m inner diameter \times 5 mm, packed with Acclaim PepMap100 C18, 5 μ m, 100 Å; LC Packings, Sunnyvale, CA). After 5 min, peptides were eluted from the trap column and separated using reversed phase chromatography (Acquity UPLC M-Class HSS T3 Column, 1.8 μ m, 75 μ m \times 250 mm, Waters, Milford, MA) by a nonlinear gradient of 0.1% formic acid in acetonitrile ranging from 3% to 41%. The high-resolution (60.000 full width at half-maximum) MS spectrum was acquired with a mass range from 300 to 1.500 m/z with automatic gain control target set to 3×10^5 and a maximum of 50 ms injection time. From the MS prescan, the 10 most abundant peptide ions were selected for fragmentation (MSMS) if at least doubly charged, with a dynamic exclusion of 30 s. MSMS spectra were recorded at 15.000 resolution with automatic gain control target set to 1×10^5 and a maximum of 100 ms injection time. Normalized collision energy was set to 28 and all spectra were recorded in profile type.

Progenesis QI for label-free quantification

Spectra were analyzed using Progenesis QI software for proteomics (Version 3.0, Nonlinear Dynamics, Waters, Newcastle upon Tyne, UK) for label-free quantification as previously described (Grosche et al., 2016) with the following changes: spectra were searched against the Swissprot mouse database (Release 2017.02, 16686 sequences). Search parameters used were 10 ppm peptide mass tolerance and 20 mmu fragment mass tolerance. Carbamidomethylation of cysteine was set as fixed modification and oxidation of methionine and deamidation of asparagine and glutamine was allowed as variable modification, with only one missed cleavage site. Mascot integrated decoy database search was set to a false discovery rate (FDR) of 1% with a percolator ion score cut-off of 13 and an appropriate significance threshold p.

Mitominer analysis

Mitochondrial assignment of proteins was assessed using the Mitominer software (Mitominer 4.0) (Smith and Robinson, 2016). Analysis was performed based on gene symbols.

Bioinformatic analysis of proteomics data

Progenesis output tables were analyzed using the Perseus software suite (version 1.5.8.7) (Tyanova et al., 2016). Log2 transformed mass spectrometry intensity values were filtered to have at least three out of four quantified values in either the WT or the mutator group. Zero values were imputed with a normal distribution of artificial values generated at 1.6 standard deviations, subtracted from the mean, of the total intensity distribution and a width of 0.3 standard deviations. This places the imputed values at the lower limit of the intensity scale, which represents detection limit of the used instrumentation. For gene annotation enrichment analysis of the data from isolated mitochondria, we used 710 proteins that were confirmed to be true mitochondrial proteins based on the Mitominer software (see above).

Gene annotation enrichment analysis was performed with the 1D annotation enrichment algorithm as previously described (Schiller et al., 2015). As gene annotations for significance tests, we used the Uniprot Keyword annotation as well as Gene Ontology terms Biological process (GO:BP), Molecular function (GO:MF) and Cellular Component (GO:CC) (Cox and Mann, 2012). In brief, it is tested for every annotation term whether the corresponding numerical values have a preference to be systematically larger or smaller than the global distribution of the values for all proteins, which is reported as normalized enrichment score. Additional pathway analysis was performed with the DAVID Bioinformatic Resources 6.8.

Cell proliferation assay

20.000 cells per cell line were seeded as triplicates in 6 well plates. After attachment of the cells overnight control wells were counted for each cell line to determine the starting cell number after cell seeding. For aspartate supplementation cells were washed with PBS and 4 mL DMEM High Glucose medium containing 10 mM aspartate was added to the wells. Cells were then counted again at day 5 of the experiment to determine the final cell number and doubling rates per day were calculated with the following formula as previously described by Sullivan et al. (2015): $\text{Proliferation Rate (Doublings per day)} = \log_2 (\text{Final cell count (day 5)} / \text{Initial cell count (day 1)}) / 4 \text{ (days)}$

Protein synthesis assay (WT versus mutator MEFs)

Nascent protein synthesis was analyzed using the Click-iT Plus OPP Protein Synthesis Assay Kit (Life Technologies, Carlsbad, CA, USA). 6.000 cells/well were seeded in black clear-bottom 96 well plates and left over night to attach to the plate. Cells were then treated for 4 h with control medium or with medium containing 100 μM cycloheximide. After the treatment, medium was removed and cells were incubated with growth medium containing 20 μM Click-iT O-propargyl-puromycin (OPP) reagent for 30 min. Afterward, OPP-containing medium was removed, cells were washed with PBS and fixed with 4% PFA for 15 min. After fixation, cells were permeabilized in 0.5% Triton X-100 in PBS for 15 min, washed twice with PBS and stained by adding 50 μl Alexa Fluor® (AF)-647 picolyl azide-containing Click-iT Plus OPP reaction cocktail per well and incubating for 30 min. Afterward, cells were washed with PBS and nuclei were stained by incubation with HCS NuclearMask Blue Stain in PBS for 30 min. Cells were washed again twice with PBS and fluorescence was measured using the LSM710 fluorescence microscope (Zeiss, Oberkochen, Germany). Protein synthesis was measured as the mean intensity of the red signal and normalized to cell number assessed by the blue NuclearMask signal.

Protein synthesis assay (aspartate treatment of mutator MEFs)

20.000 cell per mutator MEF cell line ($n = 4$) were seeded on coverslips in 6 well plates. After overnight regeneration cells were treated with 10 mM aspartate supplemented in high glucose medium for 48 h. Cells were then treated for 4 h with control medium or with medium containing 100 μM cycloheximide. After the treatment, medium was removed and cells were incubated with growth medium containing EZClick™ O-propargyl-puromycin (OPP) reagent (Biovision, Milpitas, USA) for 30 min. Afterward, OPP-containing medium was removed, cells were washed with PBS and fixed with 4% PFA for 15 min. After fixation, cells were permeabilized in 0.5% Triton X-100 in PBS for 15 min, washed twice with PBS and stained by adding 500 μl EZClick™ fluorescence azide reaction cocktail for 30 min. Afterward, cells were washed with PBS and nuclei were stained by incubation with 4'-6-Diamidin-2-phenylindol (DAPI) (Sigma-Aldrich) in PBS for 30 min. Cells were washed again with PBS and mounted on object slides with DAKO mounting medium (DAKO, Hamburg, Germany). Fluorescence was measured using the LSM710 fluorescence microscope (Zeiss).

siRNA mediated mRNA silencing

We first determined the optimal siRNA concentrations for efficient knockdown of Rpn4, p28 and Raptor (10 nM), which did not affect cell viability and proliferation. As Rpn6 is an essential proteasome subunit, we performed only a partial knockdown of this subunit (0.3 nM), which did not affect cell growth. Reverse transfection of mutator MEFs was used to deliver siRNAs. Two different siRNAs and control siRNAs were used for each of the different targets (p28: s203895+s79154; Rpn6: s87416+s87415; Rpn4: s84561+s84562, Control siRNA Negative Control #1+#2, Ambion, Thermo Fisher Scientific). Raptor knockdown was performed with one Raptor siRNA (s92713) and Control siRNA Negative Control #1. siRNAs were first incubated with Opti-MEM for 5 min at RT and 5 μ L of transfection reagent (RNAiMax, Thermo Fisher Scientific) was applied per 6 well. siRNAs were incubated with transfection reagent for further 20 min at RT. Cells were harvested in antibiotic-free medium, counted, and plated in 6 well plates. 20.000 cells per well were plated for 72 h aspartate treatment and 100.000 cells per well for 48 h of silencing without aspartate. Opti-MEM containing siRNAs and transfection reagents was added to the cells. The next morning medium was changed either with normal DMEM High glucose medium or medium containing 10 mM aspartate. Silencing efficiency was confirmed via immunoblotting of the respective proteins.

Rapamycin and aspartate cotreatment of mutator cells

Optimal concentration for rapamycin was first determined for mutator cells by assaying phosphorylation of p70 S6 kinase. At a concentration of 0.5 nM mTORC1 was specifically inhibited while mTORC2 was not affected (no decrease in the phosphorylation of Akt). Mutator cells were seeded the day before the treatment. 40.000 cells per well were used per 6 well. After overnight attachment cells were treated with 4 mL of medium containing 10 mM aspartate and 0.5 nM rapamycin for 72 h. Efficiency of mTOR inhibition was confirmed by reduced phosphorylation of p70 S6 kinase.

Bulk mRNA sequencing

300.000 cells from one representative WT and mutator MEF cell line were seeded in 6 well plates. Cells for 5 technical replicates per cell line were plated. After 48 h cells were harvested.

Strand specific, polyA-enriched RNA sequencing was performed as described earlier ([Haack et al., 2013](#)). Briefly, RNA was isolated from whole-cell lysates using the Total RNA kit (PqLab, VWR) and RNA integrity number (RIN) was determined with the Agilent 2100 BioAnalyzer (RNA 6.000 Nano Kit, Agilent). For library preparation, 1 μ g of RNA was poly(A) selected, fragmented, and reverse transcribed with the Elute, Prime, Fragment Mix (Illumina). A-tailing, adaptor ligation, and library enrichment were performed as described in the TruSeq Stranded mRNA Sample Prep Guide (Illumina). RNA libraries were assessed for quality and quantity with the Agilent 2100 BioAnalyzer and the Quant-iT PicoGreen dsDNA Assay Kit (Life Technologies). RNA libraries were sequenced as 150 bp paired-end runs on an Illumina HiSeq4000 platform. The STAR aligner (v 2.4.2a) with modified parameter settings (–twopass-Mode = Basic) was used for split-read alignment against the human genome assembly hg19 (GRCh37) and UCSC known gene annotation. To quantify the number of reads mapping to annotated genes we used HTseq-count^o (v0.6.0) ([Anders et al., 2015](#)). FPKM (Fragments Per Kilobase of transcript per Million fragments mapped) values were calculated using custom scripts. Normalized dataset was analyzed using the Perseus Software as described in the proteomics section.

Cotreatment of bortezomib and pyruvate/metformin

40.000 WT MEFs/well or 50.000 mutator MEFs/well were seeded into 24-well plates. The next day, medium was exchanged with 1 mL of medium containing 1 mM pyruvate, 5 mM metformin or a combination of both. Cells were incubated for 24 h. Following, Bortezomib (stock concentration: 2.6 mM, dissolved in water) was added to the wells in different concentrations as indicated in the respective figure. Cells were then incubated for further 48 h, harvested and analyzed.

Cell viability assay (MTT)

Cellular viability was measured using the 2,5-diphenyltetrazolium bromide (MTT) assay. 40.000 WT MEFs/well or 50.000/well mutator MEFs were seeded into 24-well plates. Cells were grown for 24 h and medium was exchanged to 1 mL treatment or control medium as indicated in the figures. After treatment, 200 μ L of freshly prepared thiazolyl blue tetrazolium bromide solution (5 mg/ml in PBS) (Sigma-Aldrich, St. Louis, MO) was added to each well and cells were incubated for 30 min at 37°C. The supernatant was aspirated, and blue crystals were dissolved in isopropanol + 0.1% Triton X-100. 200 μ L of the colored solution were transferred in a 96-well plate. Each sample was measured in duplicates. Absorbance was measured at 570 nm using a Tristar LB 941 plate reader.

Live/dead staining with annexin V/PI

Induction of apoptosis or necrosis was analyzed by staining cells with an Annexin V antibody and Propidium iodide (PI). Cells were seeded into 6-well plates and grown for 24 h. Cells were then treated with Bortezomib for 24 h. After the treatment, cells were trypsinized, washed twice with PBS and resuspended in 100 μ L Annexin V binding buffer. 5 μ L anti-Annexin V-FITC (BD Biosciences, San Jose, CA) and 10 μ L PI staining solution were added and cells were incubated for 15 min at room temperature in the dark. After the incubation time, 400 μ L Annexin V binding buffer were added and sample fluorescence was measured by flow cytometry analysis using the Becton Dickinson LSRII and analyzed using FlowJo software (version 7.6.5).

QUANTIFICATION AND STATISTICAL ANALYSIS

Data are depicted in the figures as mean \pm SEM. All statistical analysis was performed using GraphPad Prism software (Version 5+7, GraphPad, San Diego, CA, USA). Statistical tests were applied to all experiments where applicable. The applied statistical tests are indicated in the respective figure legends. Student's unpaired t test was used to determine significance between WT and Mut MEFs. Student's paired t test was used to determine significant differences when different mutator cell lines were treated with aspartate or pyruvate. The one sample t test was used to determine significance when native gel immunoblotting was performed with one single cell line or different mutator cell lines to eliminate signal intensity differences between replicates or individual mutator cell lines. Significance was indicated in the figures as *: $p < 0.05$, **: $p < 0.01$ or ***: $p < 0.001$. Data that are not labeled with a star did not reach statistical significance. Statistical analysis of the respective experiments was performed as explained in the figure legends.

Supplemental Information

Mitochondrial Regulation of the 26S Proteasome

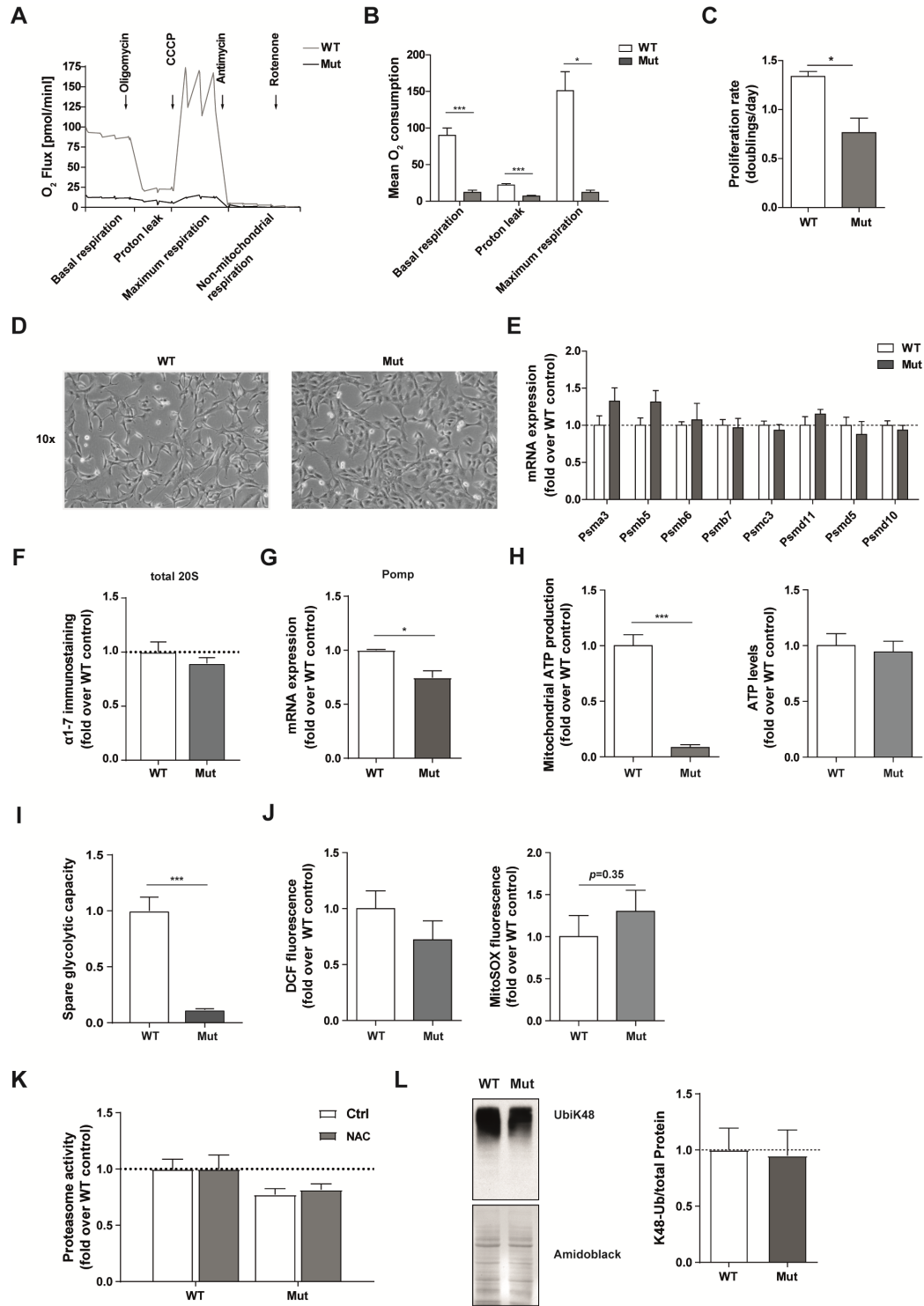
Thomas Meul, Korbinian Berschneider, Sabine Schmitt, Christoph H. Mayr, Laura F. Mattner, Herbert B. Schiller, Ayse S. Yazgili, Xinyuan Wang, Christina Lukas, Camille Schlessner, Cornelia Prehn, Jerzy Adamski, Elisabeth Graf, Thomas Schwarzmayer, Fabiana Perocchi, Alexandra Kukat, Aleksandra Trifunovic, Laura Kremer, Holger Prokisch, Bastian Popper, Christine von Toerne, Stefanie M. Hauck, Hans Zischka, and Silke Meiners

1

Supplemental information

2

Figure S1: related to Figure 1



3

4

5

6 **Figure S1: related to Figure 1**

7 (A) Mitochondrial oxygen flux monitored over time at base line condition, after addition of
8 oligomycin (determining proton leak), CCCP (assessing maximal respiration), or antimycin A and
9 rotenone (assaying non-mitochondrial respiration) as analyzed by the Seahorse XF analyzer.
10 Curves show mean values from three independent wildtype (WT) and four independent
11 mutator (Mut) cell lines. (B) Mean oxygen consumption rates in WT (n=3) and mutator (n=4)
12 cells. Bar graphs show mean \pm SEM. Significance was determined using two-way ANOVA with
13 Bonferroni multiple comparison test. (C) Proliferation rates of WT (n=3) and mutator (n=4) cell
14 lines were determined by counting cells at day 1 and day 5 after seeding of the cells. Doublings
15 per day were then calculated as explained in the methods part. Bar graphs show mean \pm SEM.
16 Significance was determined using student's unpaired t-test. (D) Representative images show
17 cellular morphology of WT and mutator MEFs. Magnification: 10x. (E) RT-qPCR analysis of
18 proteasome subunit mRNA expression in WT (n=3) and mutator (n=4) cells. Data represent
19 mean \pm SEM relative to WT control. Statistical test: two-way ANOVA with Bonferroni multiple
20 comparison test. (F) Quantification of amounts of total 20S complexes in WT and mutator cells
21 as resolved by blotting of native gels and immunostaining for the 20S subunits α 1-7. Bar graph
22 shows combined signals for 30S, 26S and 20S related to WT controls. Significance was
23 determined using student's unpaired t-test. (G) RT-qPCR analysis of Pomp mRNA expression in
24 WT (n=3) and mutator (n=4) cells. Data represent mean \pm SEM relative to WT control. Statistical
25 test: unpaired t-test. (H) Relative mitochondrial ATP production (oligomycin sensitive
26 respiration) in WT (n=3) and mutator (n=4) cells as analyzed by the Seahorse XF analyzer.
27 Relative cellular ATP levels in WT (n=3) and mutator (n=4) cells as measured by a luciferase-

based assay. (I) Extracellular acidification rate (ECAR) was measured using the Seahorse XF analyzer to determine the spare glycolytic capacity in WT (n=3) and Mut MEFs (n=4). Values were normalized to the mean of WT controls. Significance was determined using student's unpaired t-test. (J) Cellular ROS was measured using H₂DCFDA staining and flow cytometry in WT (n=2) and mutator (n=2) cell lines. Flow cytometry analysis of WT (n=3) and mutator (n=4) cell lines stained with MitoSOX Red for detection of mitochondrial superoxides. Data represent mean±SEM relative to WT. Significance was determined using student's unpaired t-test. (K) CT-L proteasome activity in WT (n=3) and mtDNA mutator (n=4) MEFs after treatment with control or 5 mM NAC-containing medium for 2 h. Bars show mean±SEM. Values were displayed as fold change relative to WT. (L) Analysis of ubiquitinated proteins in WT and mutator cells. Representative Western blots of UbiK48-linked proteins. Bar graphs show Amido black normalized levels of UbiK48-linked proteins in WT (n=3) and mutator (Mut) cell lines (n=4) (mean±SEM). Significance was determined using student's unpaired t-test.

Figure S2: related to Figure 2

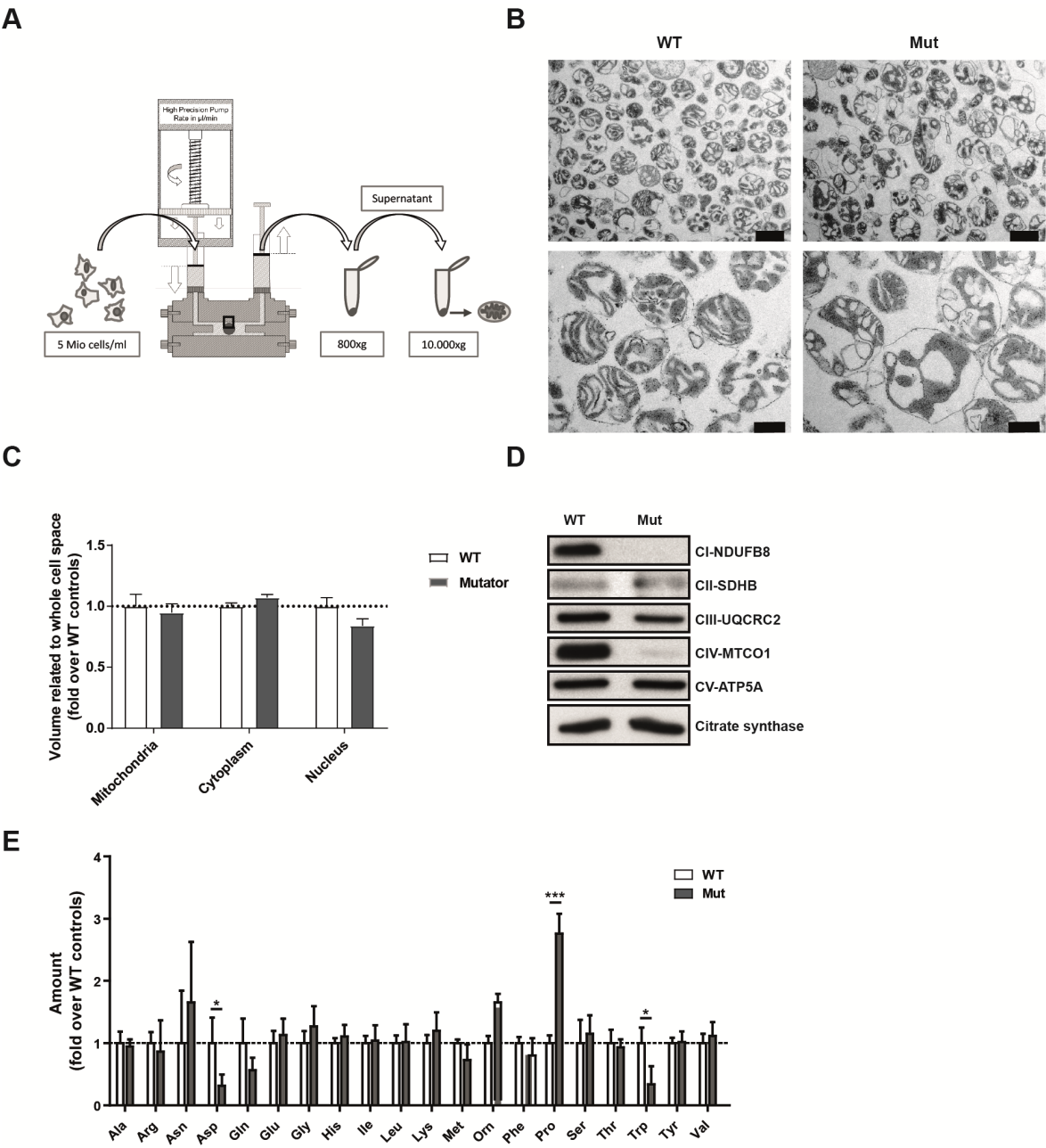


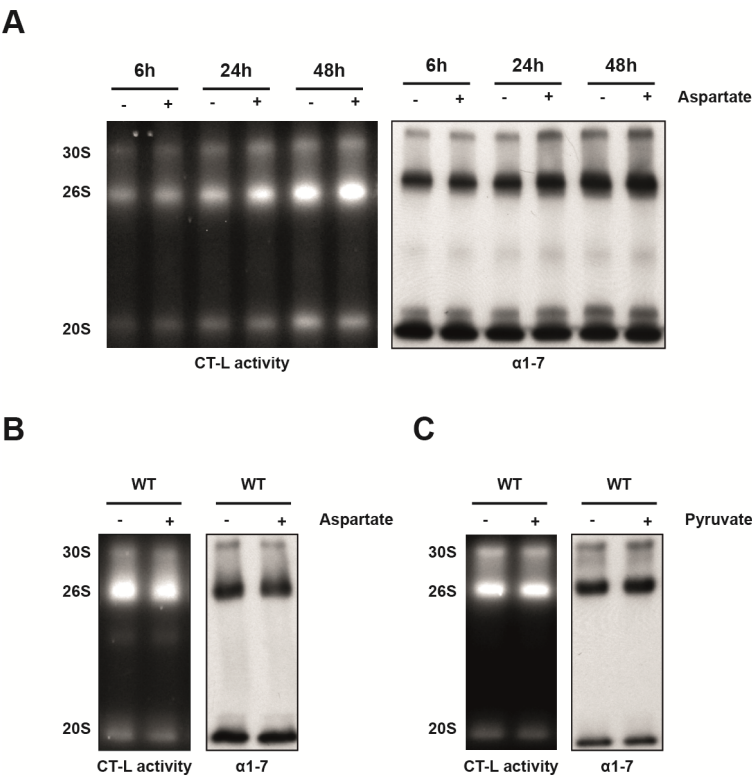
Figure S2: related to Figure 2

(A) Scheme of the mitochondrial isolation procedure. A high precision pump ensures, via gastight syringes, the continuous sample delivery in a constant rate to the “Balch-

homogenizer". Cell breakage occurs upon passage through a defined clearance (square), which is adjusted by selecting tungsten carbide balls of different diameters. The cell homogenate is collected in a second syringe and transferred to a 2ml Eppendorf cup for differential centrifugation. (B) Representative electron microscopy images of mitochondria isolated from one WT and mutator cell line. Scale bar: upper panel 1 μm , lower panel 500 nm. (C) Proportion of mitochondrial volume was quantified as described by Hacker and Lucocq (Hacker and Lucocq, 2014). In total, 30 electron micrographs (1000x magnification) from three wildtype clones (two technical replicates, each) and 43 electron micrographs (1000x magnification) from four mutator clones (two technical each) were used for quantification. Data represent mean \pm SEM relative to WT controls. Statistical test: student's unpaired t-test. (D) Representative Western blot analysis of single respiratory chain complex subunits in mitochondria isolated from one WT and mutator cell line. Four independent isolations were used for Western blots. Citrate synthase served as a loading control. (E) Quantification of the amount of 20 amino acids in WT (n=3) and mutator (n=4) cells. 6 replicates were measured for each cell line and the respective values were normalized to the cell number of each cell line. Data represent mean \pm SEM relative to WT controls. Statistical test: student's unpaired t-test.

66

67 **Figure S3: related to Figure 3**



68

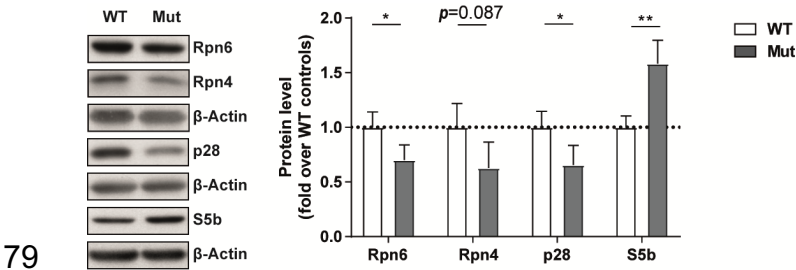
69 **Figure S3: related to Figure 3**

70 (A) Representative native gel analysis of active proteasome complexes in cell lysates from one
71 mutator cell line treated with 10 mM aspartate for 6 h, 24 h and 48 h. Chymotrypsin-like (CT-L)
72 substrate overlay assay and immunoblotting for 20S α 1-7 subunits is shown. (B+C) Native gel of
73 active proteasome complexes in cell lysates from WT cells (n=3) treated with 10 mM aspartate
74 or 1 mM Pyruvate for 72 h. Chymotrypsin-like (CT-L) substrate overlay assay and
75 immunoblotting for 20S α 1-7 subunits is shown.

76

77

78 **Figure S4: related to Figure 4**



80

81

82 **Figure S4: related to Figure 4**

83 Western blot analysis of 26S proteasome assembly factor expression in WT and mutator cells.

84 β-Actin was used as a loading control. Densitometric analysis shows mean±SEM from three WT

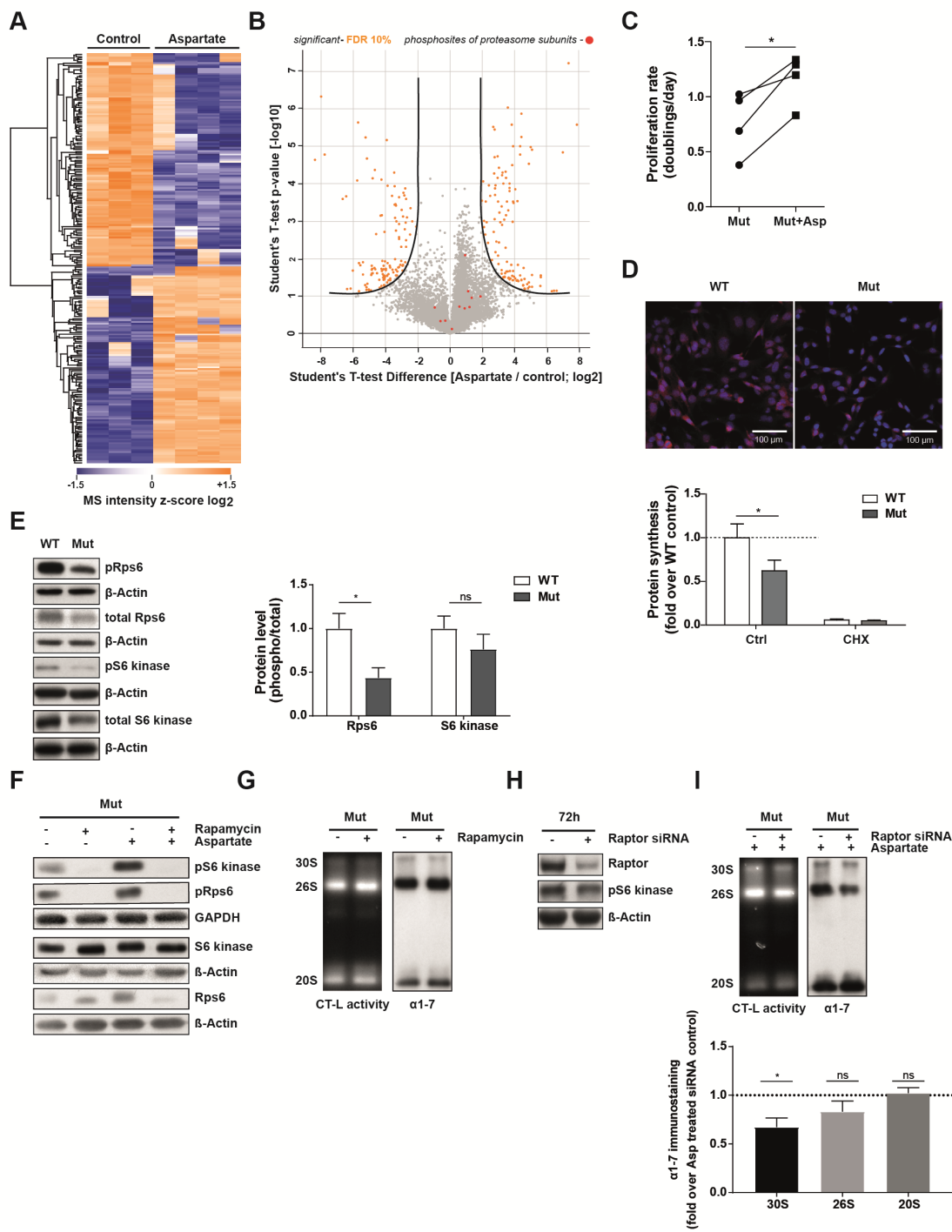
85 and four mutator cell lines. Significance was determined using student's unpaired t-test.

86

87

88

89 **Figure S5: related to Figure 5**



90

91 **Figure S5: related to Figure 5**

92 (A) Heatmap of 233 phosphosites significantly regulated by aspartate treatment compared to
93 non-treated controls. Each row corresponds to a single distinct phosphosite. Rows are ordered
94 according to unsupervised hierarchical clustering (Pearson correlation of z-score), after
95 imputation to replace missing values. (B) The depicted volcano plot shows significantly altered
96 phosphorylation sites relative to controls with a 10 % FDR. Phosphosites of proteasome
97 subunits are shown in red. (C) Proliferation rates of mutator (n=4) cell lines treated with 10 mM
98 aspartate were determined by counting cells at day 1 and day 5 after seeding of the cells.
99 Doublings per day were then calculated as explained in the methods part. Graph shows
100 increase for each mutator cell line after aspartate supplementation. Significance was
101 determined using student's paired t-test. (D) Representative fluorescence images showing
102 nascent protein synthesis (red signal) and cell nuclei (blue signal) in WT (n=3) and mutator (n=4)
103 cells. (Cycloheximide CHX) treatment with 100 μ M for 4 h served as a negative control. Scale
104 bar: 100 μ m. Graph shows mean \pm SEM relative to WT for Ctrl and CHX treated samples.
105 Statistical test: Two-way ANOVA with Bonferroni multiple comparison test. (E) Analysis of
106 mTOR signaling in WT (n=3) mutator (n=4) cells. Representative Western blots of total and
107 phosphorylated levels of p70 S6 kinase and S6 ribosomal protein (Rps6). Bar graphs show β -
108 Actin normalized phospho-protein levels related to total levels of the respective protein in WT
109 and mutator cells (Mean \pm SEM). Significance was determined using student's unpaired t-test. (F)
110 Analysis of mTOR signaling upon treatment with 0.5 nM rapamycin and 10 mM aspartate for 72
111 h in one mutator cell line. Representative Western blots of total and phosphorylated levels of
112 p70 S6 kinase, S6 ribosomal protein (Rps6). GAPDH and β -Actin was used as a loading control.
113 (G) Representative native gel analysis of active proteasome complexes in cell lysates from one

114 mutator cell line upon rapamycin treatment (0.5 nM) for 72 h. Chymotrypsin-like (CT-L)
115 substrate overlay assay and immunoblotting for 20S α 1-7 subunits is shown (H) Protein levels
116 of Raptor and phospho S6 kinase after aspartate supplementation and siRNA mediated Raptor
117 silencing in one mutator cell line (n=4 independent experiments). (I) Representative native gel
118 analysis of active proteasome complexes in cell lysates from one mutator cell line upon 72 h
119 treatment with 10 mM aspartate and siRNA mediated Raptor silencing. Chymotrypsin-like (CT-
120 L) substrate overlay assay and immunoblotting for 20S α 1-7 subunits is shown. Densitometric
121 analysis shows mean \pm SEM of fold change over control from four independent experiments.
122 Significance was determined using the one sample t-test.

123

124

Figure S6: related to Figure 6

A

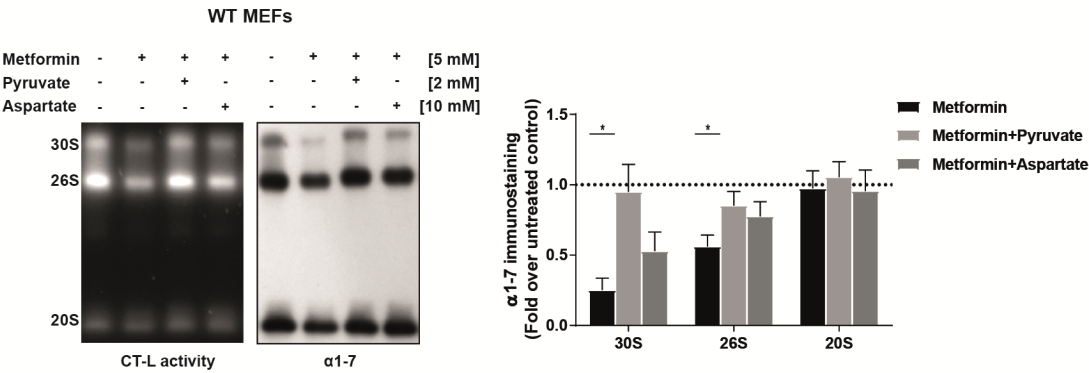
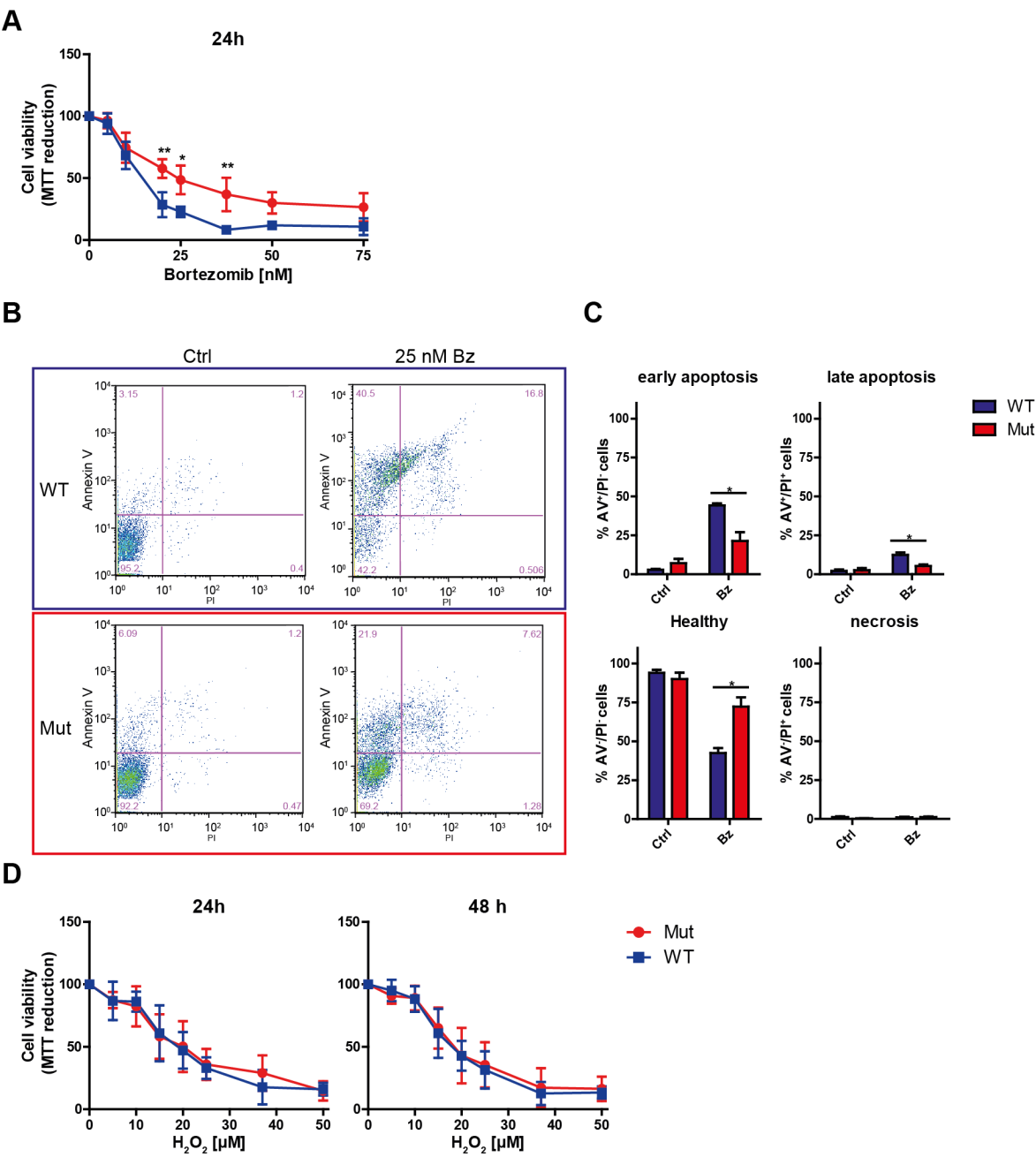


Figure S6: related to Figure 6

Representative native gel analysis of active proteasome complexes in cell lysates from one WT MEF cell line cotreated with 10 mM aspartate or 1 mM pyruvate together with 5 mM metformin for 72 h. Chymotrypsin-like (CT-L) substrate overlay assay and immunoblotting for 20S $\alpha 1-7$ subunits is shown. Bar graphs represent mean \pm SEM relative to respective untreated WT MEF cell line (n=4 independent experiments). Significance was determined using one sample t-test.

136

137 **Figure S7: related to Figure 7**



138

139

140

141 **Figure S7: related to Figure 7**

142 (A) MTT cellular viability assay of WT (n=3) and mutator (n=4) MEFs treated with increasing
143 doses of the proteasome inhibitor Bortezomib for 24 h. Values were normalized to the solvent-
144 treated control (0 nM Bortezomib) and are displayed as mean+SEM. Significance was
145 determined using two-way ANOVA with Bonferroni multiple comparison test. *:p< 0.05, **:p<
146 0.01, ***:p< 0.001. (B) Representative flow cytometry analysis of Annexin V and PI staining of
147 WT and mutator MEFs treated with either solvent or 25 nM Bortezomib (Bz) for 24 h. (C)
148 Quantification of Annexin V/PI staining in WT (n=3) and Mut (n=4) cells. Cells were classified as
149 healthy (Annexin V⁻/PI⁻), early apoptotic (Annexin V⁺/PI⁻), late apoptotic (Annexin V⁺/PI⁺), or
150 necrotic (Annexin V⁻/PI⁺). Bar graphs show mean+SEM. Significance was determined using
151 student's t-test. *:p< 0.05. (D) Cellular viability of WT (n=3) and mutator (n=4) MEFs treated
152 with increasing concentrations of H₂O₂ for 24 or 48h. Values were normalized to the 0 μM H₂O₂-
153 treated group and are displayed as mean+SEM.